2021

Influence of Iceberg-Discharge Events on the Climate and Circulation of the Central North Atlantic Ocean During the Last Glaciation

Ava McIlvaine

Influence of Iceberg-Discharge Events on the Climate and Circulation of the Central North Atlantic Ocean During the Last Glaciation

A Thesis Presented

by

Ava C. McIlvaine

Under the Supervision of

Research Advisor: Dr. Jerry F. McManus, Dep. of Earth and Env. Science, LDEO - Columbia
Thesis Advisor: Dr. Branwen Williams, Dep. of Env. Science, Keck Science Department

To the Keck Science Department
Of Claremont McKenna, Pitzer, and Scripps Colleges

In partial fulfillment of
The degree of Bachelor of Arts

Senior Thesis in Environmental Science
May 3rd, 2021

Abstract

The repeated occurrence of episodic iceberg-discharge events and abrupt climate change in the North Atlantic Ocean is well-documented for the late Quaternary period. However, much of the evidence for these periods known as Heinrich Events comes from the subpolar region, where deposition can be dominated by ice-rafted debris (IRD) and overwhelm other oceanographic and climatic indicators. Thus, the following analysis of coarse sediment from Integrated Ocean Drilling Program (IODP) Core Site U1313 (41°0.0'N, 32°57.42'W) evaluated ocean cooling related to ice-rafting, water mass migration, and climate change over the approximate last 100,000 years. Site U1313 is located near the North Atlantic Ocean's subpolar-subtropical gyre boundary and has the potential to enhance the existing record of Heinrich events both temporally and spatially. IODP Site U1313 (reoccupation of Deep Sea Drilling Project (DSDP) Site 607) is situated on the western flank of the Mid-Atlantic Ridge (3413 m) at a climatically sensitive location that is currently bathed at depth by North Atlantic Deep Water (NADW). Investigation into the core's coarse sediment (>150 µm fraction) documented the presence of polar planktonic foraminifera species *N. pachyderma (sinistral)*, subpolar species *T. quinqueloba*, transitional species *G. inflata*, and IRD, indicating the possible past extension and retraction of colder poleward waters into the temperate central North Atlantic Ocean. The addition of Site U1313's reconstructed regional signal into the complex history of the North Atlantic contributes to our current understanding of the strength, timing, and spatial extent of past iceberg-discharge events. Site U1313 shows that Heinrich Events repeatedly influenced the central North Atlantic Ocean and were associated with nuances in the region's surface ocean conditions. This study's high-resolution record draws our attention back to the influence of changing Sea Surface Temperatures (SSTs) on the biogeochemical composition of the water column. Core U1313 expands upon existing research into the impacts of climate variability in the North Atlantic by providing new insight from the subtropical-subpolar transitional zone into the role of the cryosphere and surface ocean circulation during periods of abrupt climate change in the last glaciation.

Table of Contents

Acknowledgements
First and foremost, I would like to thank the scientific community at Lamont-Doherty Earth Observatory for making this research experience possible during the COVID-19 pandemic. Despite the remote nature of my research, the leadership, organization, and kindness exhibited by the LDEO staff made me feel like I was a part of the Lamont community. A very special and heartfelt thank you to my research advisor Dr. Jerry F. McManus for his unwavering support and guidance throughout this process. Learning how to pick foraminifera and ice-rafted debris over a Zoom call could have been a recipe for disaster, but his patience and infectious curiosity made this research one of the best experiences of my life. I must also take the time to properly thank my senior thesis advisor Dr. Branwen Williams for welcoming me into the wonderful world of climate science and oceanography as an undergraduate. She has been a steadfast role model to me over the past four years, and I strive to emulate her sharp intelligence, amazing time-management skills, and overall poise in my work. Thank you to my friends and family for allowing me to turn my house into a mad scientist's laboratory over the past year, and more importantly, for your unconditional love and support. I quite simply would not be where I am today without you. Further thanks to the IODP Expedition 306 Scientists (Channell et al., 2006) and LDEO staff involved in Site U1313's preliminary core processing. This research was funded by the National Science Foundation and was made possible through the Research Experiences for Undergraduates (REU) program.

I. INTRODUCTION

A. Modern Circulation Profile of the North Atlantic Ocean

The surface circulation of the North Atlantic Ocean is comprised of two major oceanographic systems known as the subtropical and subpolar gyres. These gyres are large bodies of rotating water masses whose circulation is driven by the interaction of wind with the surface ocean and basin-wide differences in temperature and salinity (Daniault et al., 2016). Surface gyre currents can vary in strength and depth, but mainly affect the upper 100 meters (Stouffer et al., 2006). However, strong boundary currents can reach much greater depths. Together, the gyres are responsible for the oceanic circulation and atmospheric regulation of the North Atlantic.

The North Atlantic subtropical gyre rotates in a clockwise direction (anticyclonic motion) and forms under a high-pressure system (Appendix A; Univ. of Washington, 2002). It is located between the polar and equatorial latitudes and pushes entrained water towards the gyre center due to the net movement of Ekman transport. The central collection of water then sinks due to continual convergence. The subtropical gyre is a collection of warm, nutrient-poor water from the subtropics that is bounded by the Gulf Stream to the west and the cold Canary Current to the east (Figure 1; Gong et al., 2015). The subtropical gyre is important for modern climate dynamics as the Gulf Stream, which later travels across the Atlantic as the North Atlantic Drift current (NAC), transports heat and moisture to the northeast high latitudes (Pflaumann et al., 2003). The NAC simultaneously turns southward at the subtropical gyre's eastern side and forms the Canary Current.

The majority of the NAC joins the Norway Current or the Irminger Current near Greenland. The Irminger is a relatively warm and salty current that fuels the counterclockwise

(cyclonic) rotation of the subpolar gyre (Katsman et al., 2004; Marzocchi et al., 2015). The subpolar gyre forms under areas of low atmospheric pressure and its rotation pulls deeper waters to the surface. The strength and spatial extent of the subpolar gyre is impacted by the northward transport of heat by the NAC and the input of cold, fresh water from the glaciers surrounding the North Atlantic Ocean (Naafs et al., 2013). The subpolar gyre's strong interaction with the atmosphere influences the climate of the North Atlantic's high-latitude regions (around 60°N). Its role in the thermohaline circulation pulls heat from temperature latitudes poleward and powers the Atlantic Meridional Overturning Circulation (AMOC) (Lehman & Keigwin, 1992). Specifically, modeled variations in the strength of the Irminger Current suggest that its ability to sequester heat into the Labrador Sea influences the rate of deep water formation in the North Atlantic (Katsman et al., 2004). Deepwater formation is part of AMOC and creates an important water mass known as the North Atlantic Deepwater (NADW) that currently bathes Site U1313 at depth (Appendix C). Once the current leaves the Labrador Sea, it is recycled southward, and the North Atlantic gyre system begins again.

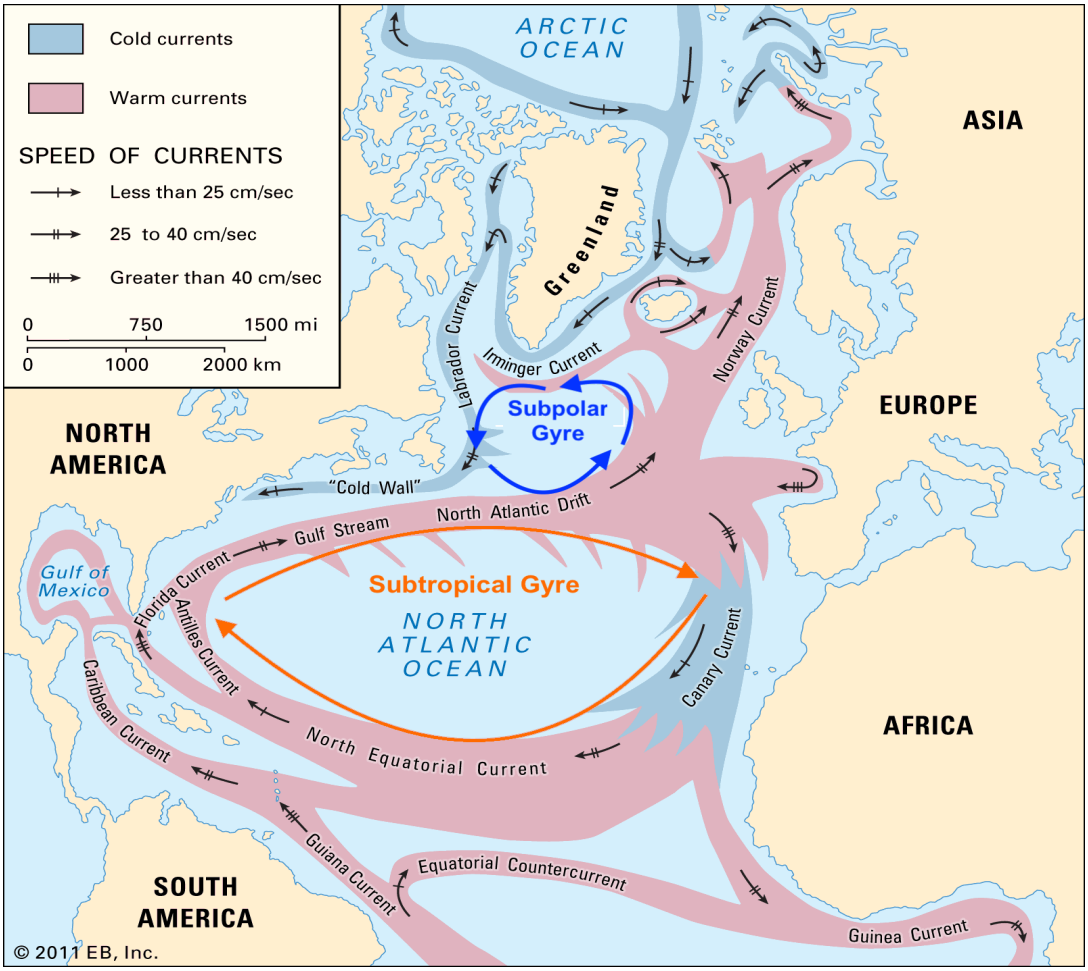

Figure 1. Simplified ocean circulation model of the major gyre systems in the modern North Atlantic Ocean. The net flow of both the subtropical and subpolar gyres is highlighted in orange and blue respectively. Image modified from Cenedese & Gordon (2011).

B. Glacial Circulation Profile of the North Atlantic Ocean

The difference in the temperature, salinity, and distribution of distinct water masses in the North Atlantic Ocean varied between recent glacial and interglacial conditions (Ruddiman 1977a, 1977b; Naafs et al., 2011; Hemming, 2004). Sediment core records and computer modeling efforts reconstructed shifts in the arctic front over the past glacial and deglacial periods (~75,000 B.P to present Holocene) potentially due to variations in the circum-Atlantic continental ice sheets, the North Atlantic Drift current, and deep water formation (Ruddiman, 1977b; CLIMAP, 1981; McManus et. al, 2002; Marchal et al., 2016; Pflaumann et al., 2003; Keigwin & Lehman, 1994). The arctic front marks the boundary between the subpolar and

subtropical gyres, and LGM reconstructions suggest it may have shifted south (36°- 42°N) during glacial conditions (see Appendix D-E for LGM model reconstructions; CLIMAP, 1981; Pflaumann et al., 2003).

The Last Glacial Maximum (~21,500 B.P) is an excellent period to compare the major differences between the glacial oceanographic and climatic profiles of the North Atlantic to modern conditions (CLIMAP, 1981; Pflaumann et al., 2003). Most studies agree that there were significant changes in the gyre distribution during the last glaciation, but the magnitude and type of change is less consistent between model interpretations (Ruddiman, 1977b; CLIMAP, 1981; Pflaumann et al., 2003). Specifically, reconstructions of the net flow of the glacial subpolar gyre disagree. Some reconstructions state there was an anticyclonic subpolar gyre during the LGM and others state it had a net cyclonic flow throughout the glacial period and reflected modern circulation. The conflicting results may be due to a difference in the studies' timescales (~18,000 B.P versus 127,000 – 11,000 B.P); this study is more closely associated with the glacial-interglacial resolution of the second interpretation. Therefore, the remainder of this research assumes net cyclonic flow in the subpolar and net anticyclonic flow in the subtropical gyres during the last glaciation (Figure 2; Ruddiman, 1977b).

The location of the arctic front gyre boundary (SST 8°-20°C) indicates how the glacial surface ocean differed from today. The subpolar gyre is bounded to the south by the warm North Atlantic Drift current which shifts during colder climates and alters the gyre distribution in the northern and central North Atlantic (Appendix B, D, E; Marzocchi et al., 2015). The exact mechanisms behind the extension and retraction of cold polar waters are still under investigation, but changes in the stability of the Atlantic Meridional Overturning Circulation (AMOC), continental glaciers, and the NAC's northward heat transport are likely responsible (McManus et

al., 1996; McManus et al., 1999; Keigwin & Lehman, 1994). Interestingly, the peak extent of continental ice storage (and iceberg release) into the North Atlantic (~20,000 B.P) is correlated with the southward migration of the arctic front around 18,000 B.P (Appendix F, G; Ruddiman, 1977b; Pflaumann et al., 2003). However, this is likely a correlation between the atmospheric control on the growth of continental glaciers and not evidence that increased iceberg propagation is solely responsible for the arctic front's migration (McManus et al., 1999; Hemming, 2004). A combination of cold global temperatures and potentially weakened circulation in the subpolar North Atlantic is a more probably control over the distribution of cold-water masses (McManus et al., 2004).

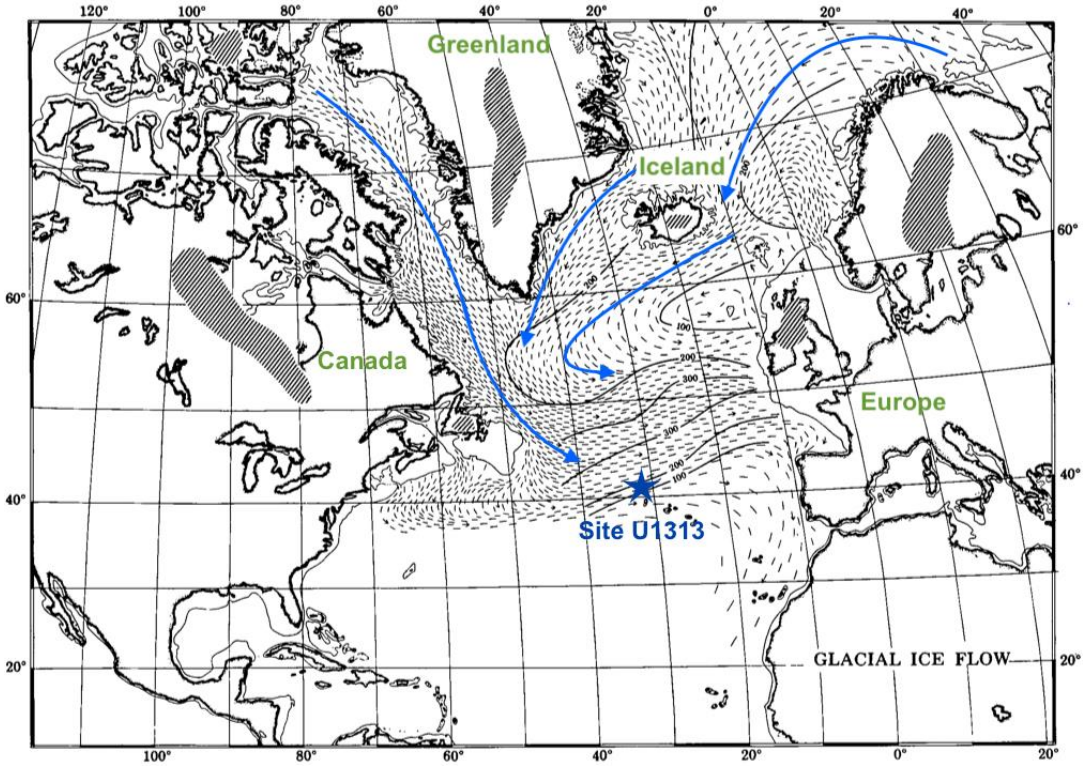

Figure 2. Inferred cyclonic circulation of the subpolar gyre in the North Atlantic Ocean based on the mean distribution of ice-rafted debris during glacial periods. Major delivery pathways for icebergs based on the presence of IRD in multiple sediment cores from 40°-65°N marked with blue arrows (Ruddiman, 1977b). Site U1313 is located just beyond the main glacial depositional axis of icebergs.

C. Reconstructing the Past with Sedimentary Proxies

Sedimentary proxies in ocean sediments are one of the most reliable methods for

reconstructing past climate variability. Sedimentary proxies are physical materials that record a past chemical, biological, or climatic signal that can be reconstructed with laboratory analysis (Heinrich, 1988; Bond et al., 1993; Broecker et al., 1993). The reconstruction of this signal is not an exact measurement of the paleo-signal, but it can be correlated to a specific environmental change or condition. Some proxies are highly reflective of their original signal, like gases trapped in ice cores, whereas other proxies, like foraminifera shells, are more distanced from their environmental signal. The strength of a study's interpretations, if based on paleoclimate proxies, is affected by the proximity of this resource to its original signal.

This study analyzed four surface water sedimentary proxies to estimate the climate (Sea Surface Temperature, SST) and potential influence of dominant circulation patterns in the central North Atlantic for the past ~100,000 years. The first three proxies consist of the planktonic foraminifera species *Neogloboquadrina pachyderma (sinistral, left-coiling), Turborotalita quinqueloba,* and *Globorotalia inflata.* These species are well-known sedimentary proxies and have strong, predictable correlations to sea surface temperatures and water mass distributions in the past and present North Atlantic (Appendix I; Bé & Tolderlund, 1971; Ruddiman, 1977b; Bé & Hutson, 1977; Heinrich, 1988; Bond et al., 1993; Bond & Lotti, 1995; Hemming, 2004). These species float within the water column and reflect the migration of their required environmental conditions (Kipp, 1976). Temperature, salinity, water density, currents, nutrients, water turbidity, light, pH, carbon, and oxygen concentrations are all variables that affect the growth of planktonic foraminifera (Bé & Hutson, 1977). The relative abundance of foraminifera within a sediment sample (>150μm fraction) reconstructs a representative image of both the species composition and oceanographic conditions of a specific water parcel (Kipp, 1976).

Ice-rafted debris is the fourth sedimentary climate proxy included in this research. Ice-rafted debris or IRD is a proxy for the release of sediment-bearing icebergs from continental icesheets and their passive drift through the North Atlantic's gyre circulation system (Ruddiman, 1977a, 1977b; Broecker et al., 1993). Mapping changes in the timing and amount of iceberg-discharge into the North Atlantic is important because it is related to significant shifts in the ocean basin's climate, circulation, and interaction with the atmosphere (Heinrich, 1988; Hemming, 2004).

i. Planktonic Foraminifera Proxies

The relative abundance of *Neogloboquadrina pachyderma (sinistral, left-coiling)* has a close relationship with the distribution of polar surface waters (Figure 3) (Appendix H) (Bé & Tolderlund, 1971; Kipp, 1976). Past investigations into North Atlantic marine core records have consistently found that sediments from periods with a high concentration of IRD (Heinrich Layers) were dominated by *N. pachyderma (s)* shells and indicated the presence of polar waters at that site (Heinrich, 1988; Bond et al., 1992). Furthermore, contemporary SST analysis reveals the *N. pachyderma (s)* is often the only species found in sediments beneath surface ocean temperatures equal to or less than 7°C (Pflaumann et al., 1996; Ruddiman, 1977). These waters are restricted to the very northern regions of the modern North Atlantic and would not be present at Site U1313 today (Appendix B, Ia, Ib, Ic; World Ocean Atlas, 2005). The relative abundance of *N. pachyderma (s)* thus serves as a robust sedimentary indicator of the presence of polar water.

N. pachyderma (s) is classified as a polar species since it has a distributional maximum north of 60°N (Appendix J; Bé &Tolderlund, 1971; Kipp, 1976). *N. pachyderma (s)* may reach greater than 60% abundance under polar surface waters, but is far less common within the subtropical gyre and specifically the Gulf Stream current (between 2-50%) (Kipp, 1976; Ruddiman, 1977b). The restriction of *N. pachyderma (s)* to colder waters impacts the species' latitudinal distribution and preferred depth habitat in the water column (Bé & Tolderlund, 1971; Bé & Hutson, 1977). *N. pachyderma (s)* prefers to live at subsurface depths (below 50 meters). In some instances, the species is found deeper than 500 meters based on water column stratification (Appendix I; Bé & Tolderlund, 1971).

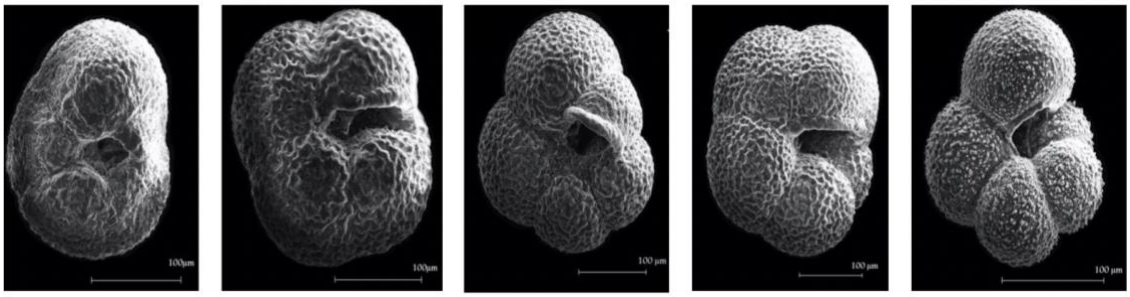

Figure 3. Representation of the five main morphotypes of *N. pachyderma (s)* taken as Scanning Electron Photomicrographs (Eynaud, 2011). Image on the far left shows the famous *N. pachyderma (s)* teardrop shape.

T. quinqueloba is the next most sensitive indicator of cold waters in the North Atlantic (Figure 4) (Appendix B, H). Similar to *N. pachyderma (s),* it has a distributional maximum north of 60°N and is found in the polar assemblage (Pflaumann et al., 1996). It is found in lower abundances because it prefers slightly warmer and shallower waters than *N. pachyderma (s)* (Kipp, 1976; Johannessen et al., 1994). *T. quinqueloba* thrives in cold to temperate waters and is classified as a subpolar species. Therefore, this species dominates the foraminiferal assemblage of sediment samples located underneath the subpolar water mass assemblage. It can be found in

waters between 1-21°C, but its greatest abundances are found in waters colder than 12°C (Bé & Tolderlund, 1971). The Gulf Stream contains 2-10% *T. quinqueloba* but its abundance increases to 10-20% as the NAC turns northeastward (Appendix I; Kipp, 1976). *T. quinqueloba* lives in the upper 10 meters of the water column and is the best paleoclimate proxy in this study for surface temperature reconstructions. However, the environmental controls on the distribution of *T. quinqueloba* are less well-understood than species like *N. pachyderma (s)*; it is only considered as a partial indicator of the location of the subpolar front (Pflaumann et al., 1996).

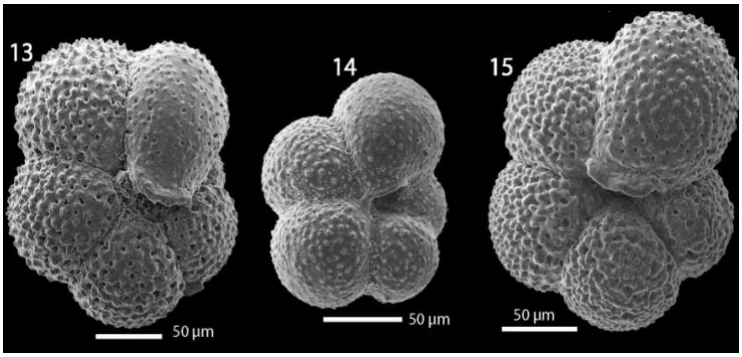

Figure 4. Representation of the three major morphotypes of the subpolar planktonic foraminifera species *T. quinqueloba* taken as Scanning Electron Photomicrographs (O'Regan et al., 2019).

The third and final planktonic foraminifera proxy analyzed in this study is the temperate water species *G. inflata.* The *G. inflata* species is native to transitional waters between the subpolar and subtropical waters of the North Atlantic (Figure 5) (Kipp, 1976). Specifically, this foram is highly concentrated in the western part of the North Atlantic Ocean and comprises more than 20% of the total foraminifera assemblage in the Gulf Stream and NAC (Bé & Tolderlund, 1971). Sediment concentrations of *G. inflata* between 10-20% indicate the presence of central and eastern North Atlantic waters, and concentrations below 2% can indicate the presence of subpolar waters (in conjunction with increased *N. pachyderma (s)* and *T. quinqueloba* abundances) (Kipp, 1976). It can overlap in temperature preference and environment with *T. quinqueloba but* is more abundant at increasingly warmer temperatures (16°-20°C). However,

this is a deeper-dwelling foraminifera species than *T. quinqueloba* and prefers subsurface depths like *N. pachyderma (s)* (Groeneveld & Chiessi, 2011). The combined analysis of the two deep-dwelling foraminifera species with the surface temperature proxy provides an estimate of paleo-temperature throughout the water column. Additionally, subsurface species *G. inflata* and *N. pachyderma (s)* compete within the same depths but live in dramatically different temperature regimes (Bé & Tolderlund, 1971). Variation in the relative abundances of these species reflects how temperatures and water masses deeper in the water column may have changed over time. Although foraminifera records do not generate as explicit of a paleoclimate reconstruction as ice-rafted debris, a combination of these proxies creates a robust methodological framework (Heinrich, 1988).

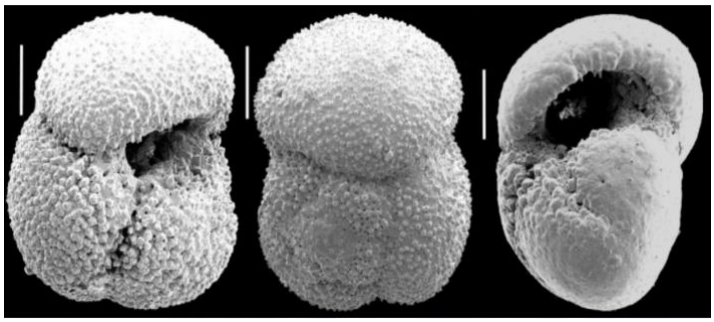

Figure 5. Representation of one primary morphotype of planktonic foraminifera species *G. inflata* taken as Scanning Electron Photomicrographs (Hayward, 2011).

ii. Ice-Rafted Debris Proxy

Glaciers create ice-rafted debris as they grind up the ground on their way towards the ocean and entrain sediments in their base. Once calved from the continental icesheet, the icebergs slowly melt and drop their sediment load to the seafloor. These iceberg 'debris rafts' leave a trail of IRD-like breadcrumbs throughout the North Atlantic Ocean that reflect the dominant circulation pattern(s) of that time. Therefore, IRD is used as a proxy for reconstructing ocean circulation pathways and the relative timing of episodic

iceberg-discharge events in the North Atlantic region (Ruddiman, 1977a; Broecker et al., 1992; Heinrich, 1988; Hemming, 2004). Silt and debris can be transported to the sea floor in many ways, but debris grains greater than 150µm were most certainly deposited by icebergs (Ruddiman, 1977b; Heinrich, 1988; Hemming, 2004). Anomalously high concentrations of IRD repeat throughout sediment core records from the polar and subpolar North Atlantic. These layers, known as Heinrich Events, reveal a complicated history of ocean, atmosphere, and cryosphere interactions that resulted in catastrophic iceberg-discharge events during the last glacial period (Ruddiman 1977b; Heinrich, 1988; Bond et al., 1992; Bond et al., 1993; Broecker et al., 1992; Broecker et al., 1993; Broecker, 1994).

Figure 6. a) Ice-rafted debris on a recently released iceberg, b) Close-up view of a sediment sample with ice-rafted debris grains and foraminifera shells from IODP Site U1308A-1H-1 (USGS, 2009; Mleneck-Vautraver in Stanley, 2017).

D. A History of Extreme Iceberg-Discharge Events in the North Atlantic

The extensive effects of episodic iceberg-discharge events on the North Atlantic Ocean during the last glacial-interglacial cycle provides a critical foundation for the modern understanding of this region's atmosphere-cryosphere-ocean interactions and global climate impact. Heinrich Events are distinct layers of anomalously high lithic fragments that demarcate past climate variability and changes in the North Atlantic's climate and circulation for the late

Quaternary period (Heinrich, 1988). During these events, armadas of icebergs released from the Laurentide and Fennoscandian ice sheets circulated throughout the subpolar gyre and left clear evidence of their oceanographic effects in sediment cores from the northern North Atlantic regions (Figure 7; Ruddiman, 1977b; Heinrich, 1988). A clear pattern of iceberg-discharge events appears on the glacial-interglacial scale, but this temporal resolution does not facilitate a detailed analysis of regionally specific oceanographic changes during Heinrich Events (Figure 7).

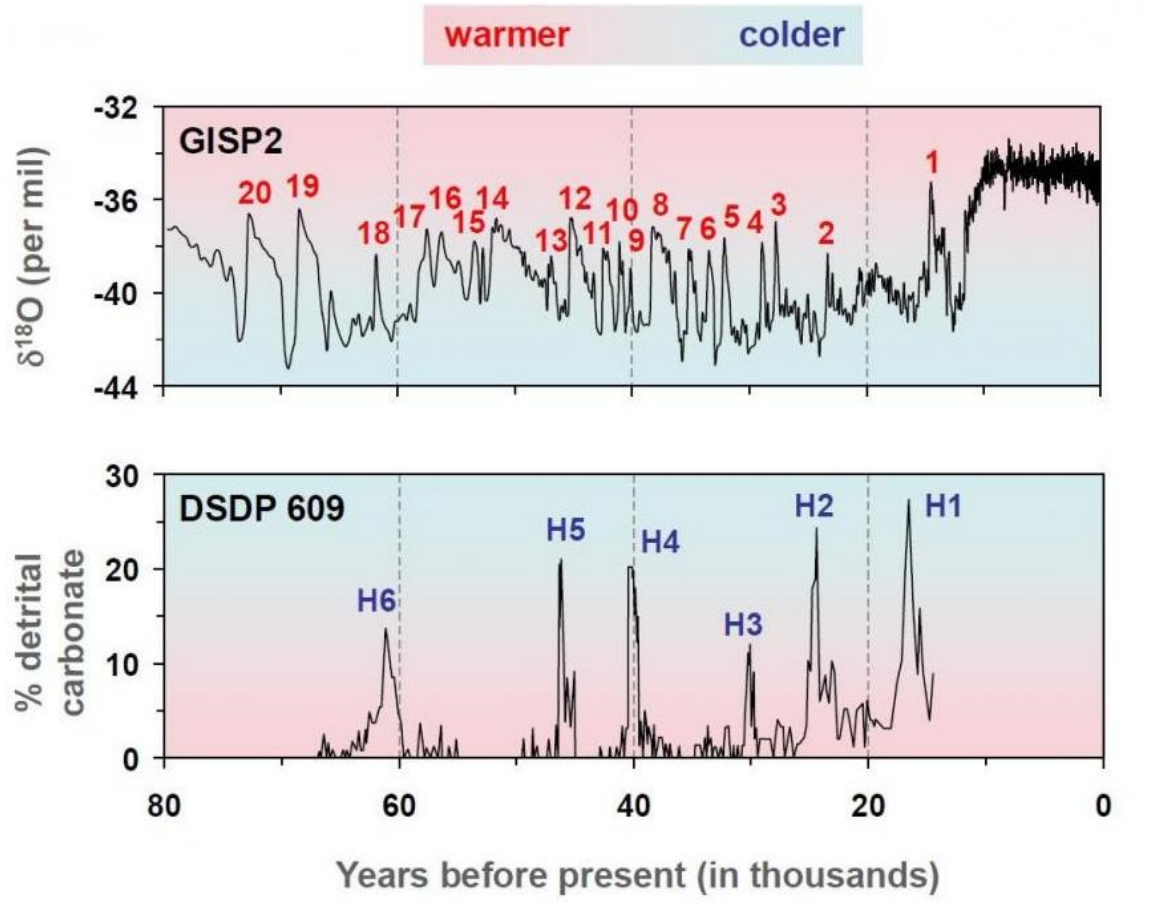

Figure 7. Comparison of percent abundance of detrital carbonate in the coarse fraction of Deep Sea Drilling Program Site 609 to the $\delta^{18}O$ of the Greenland Ice Sheet Project 2 ice core (Modified from Grootes et al., 1993). See Appendix K for the site comparison between DSDP 609 with IODP U1313.

Heinrich Events' impact on areas beyond the polar and subpolar North Atlantic is poorly resolved for the late Quaternary period. Specifically, the influence of these events on regions

outside the “ice-rafted debris belt”: a zone of maximum IRD deposition between 40°-55°N (Ruddiman, 1977b; Bond et al., 1992; MacAyeal, 1993).

Integrated Ocean Drilling Program (IODP) Site U1313 (41°0.0'N, 32°57.42'W) (3413m) is located just outside the latitudinal extent of the IRD belt, near the modern boundary of the subpolar and subtropical gyre (Figure 8). Thus, Site U1313’s paleoclimate record is uniquely posited to investigate the potential migration of the North Atlantic Ocean’s dynamic gyre system during the late glaciation. Site U1313 potentially recorded more extreme Heinrich Events while not being overwhelmed by a high concentration of IRD (as is common in cores from the IRD belt). The goal of this research is to strengthen the record of the strength, timing, and SST impacts of Heinrich Events by analyzing the combined climate signals of four sedimentary surface proxies. The study is limited spatially to achieve a higher temporal resolution.

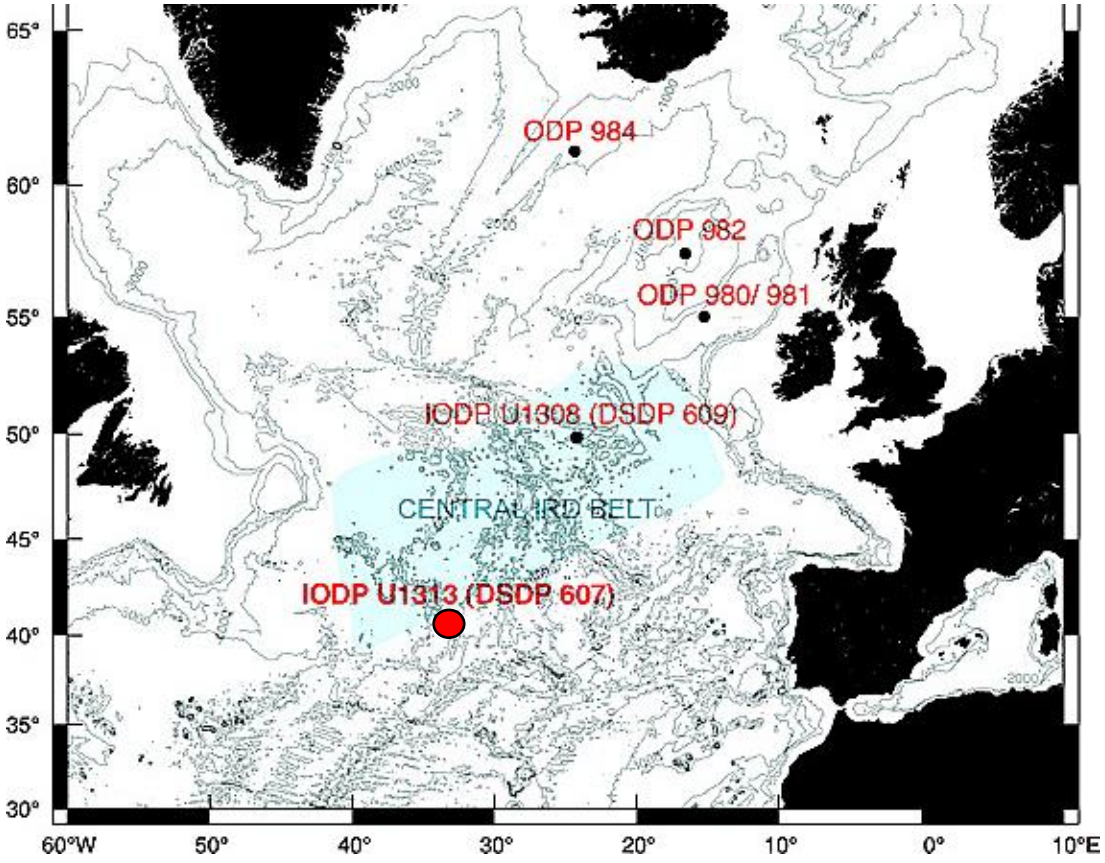

Figure 8. Location of IODP Site U1313 (41°0.0'N, 32°57.42'W) along the southern boundary of the IRD belt in the central North Atlantic Ocean (3413 m). The marine sediment core was collected by Expedition 306 Scientists (2005). IRD belt modeled by Ruddiman (1977b) and Hemming (2004). Sourced from Bolton et al. (2010).

II. METHODOLOGY

A. Sediment Sample Preliminary Processing

The Integrated Ocean Drilling Program (IODP) Site U1313 core (reoccupation of Deep-Sea Drilling Project Site 607) was divided into 2 cm intervals for sample processing (Channell et al., 2006; Lott, 2020). Samples were collected and stored to preserve the core's original sediment record. The remaining subsamples were preliminarily processed to achieve the coarse fraction (CF) for each interval. The wet sediment was dried and weighed to measure the total bulk dry sediment (grams). The bulk dry sediment was then washed and filtered through a 63μm sieve to separate out silt from the coarse fraction (Ruddiman, 1977b; Hemming, 2004). Preliminary

processing was completed once the sieved coarse fraction dried. At this point, the percent coarse fraction of each sediment subsample (CF%) can be found by dividing the CF weight (g) by the subsample's total dry weight (g) (Figure in Appendix L). See Lott (2020) for a more extensive explanation of the sediment processing methods.

B. Dry Sample Preparation for Picking and Counting

The coarse fraction subsamples were sieved once more through a 150μm sieve (Appendix M). The remaining grains (mostly foraminifera shells and mineral grains) were split in half through a sample splitter until one split reached approximately 200 – 450 grains (Pflaumann et al., 1996). This creates a representative fraction that is more manageable for counting foraminifera and IRD grains. The 200 – 450 grain subsamples were spread evenly across a small picking tray to make grain identification more reliable. The split, total planktonic foraminifera, total IRD grains, and total grains were counted under a microscope for each interval. Foraminifera shells were only counted if their species type could be easily identified (~80% of shell present). The number of foraminifera species *N. pachyderma (s)*, *T. quinqueloba*, and *G. inflata* in the subsample were recorded for all intervals. Polar species *N. pachyderma (s)* and subpolar species were recorded as estimates of cold sea surface temperature trends within the core (Lott, 2020; Pflaumann et al., 1996). *G. inflata* was recorded as an important estimate of transitional waters (Bé and Tolderlund, 1971; Kipp, 1976). The uncertainty for the counting values was calculated in Excel by taking the square root of the total amount of a variable recorded for each depth. All uncertainty values are reported in Appendix N (Taylor, 1982).

C. Subsample Grain Calculations

The final subsample grain counts were scaled using their split number (*n*) to calculate the estimated percent of either total or relative abundance of the different variables within each 2 cm study interval. The percent relative abundances of IRD, *N. pachyderma (s)*, *T. quinqueloba*, and *G. inflata* species were calculated by dividing the number of identified grains by the total amount of grains in the subsample. All calculations were done in Microsoft Excel and R Studio. A linear regression between the percent relative abundance of *N. pachyderma (s)* and IRD was run and graphed in Excel (Appendix O). All results figures were generated in R Studio (ver. 3.6.1).

D. Age Model and Planktic G. bulloides $\delta_{18}O$ Record

The age model for the upper 343 cm interval of Core U1313 was estimated with a sedimentation rate of approximately 3.5 cm/kyr (J.F. McManus, 2020, personal commun.). Each 2 cm depth interval has a resolution of approximately 571.4 years. The depth intervals were divided by the sedimentation rate to calculate their approximate age (kyrs displayed along x-axis in each figure). The estimated age model was compared to the general climate trends of the $\delta^{18}O$ *G. bulloides* record: a planktonic foraminifera species which serves as a proxy for changes in global temperature and ice volume (Kipp, 1976; Heinrich, 1988; Bolton et al., 2010; McManus et al., 1999). Heavier $\delta^{18}O$ seawater values are indicative of a colder global climate and more ice volume on land, and lighter $\delta_{18}O$ seawater values are indicative of warmer climates and less ice volume (Appendix P). The current age model estimates that the 343 cm interval extends to approximately 98,000 years ago (near the start of MIS 5c) (Ruddiman, 1977a; Lisiecki & Raymo, 2005).

E. Marine Sediment Core Resolution

The data resolution of the results presented in this analysis varied throughout the

sedimentary record. The upper 265 cm (~75.7 kyrs) of the core are well-resolved with a total of 56 data points. The lower 304-343 cm interval contains is defined by two sediment intervals (86.9 and 98.0 kyrs, respectively). This section is only partially resolved and was not used as the foundation for any of this study's major findings.

III. RESULTS

A. Heinrich Event Signals in the Ice-Rafted Debris Record

Significant iceberg-discharge events characterize core U1313 through the past 100,000 years (Figure 9). The most recent Heinrich Event (H1) occurred during the deglacial transition into marine isotope stage 1 (MIS) and was the highest concentration of ice-rafted debris (IRD) in the sediment record at 17.1 kyrs. Heinrich Event 4 (H4) was the second most intense event and was approximated at 37.1 kyrs. H1 and H4 reached similar peak IRD abundances: H1 achieved 10.03% and H4 reached 9.05% of U1313's coarse fraction. Heinrich Event 6 was estimated as the small IRD peak at 62.9 kyrs to 4.83% CF. Heinrich Event 7 or the Ruddiman Depositional Transition (RDT) is the oldest IRD peak in the core at 75.1 kyrs to 4.40% CF (Ruddiman, 1977a, 1977b). The strength and timing of Heinrich Event signals were quantitatively defined as strong, weak, and/or offset as follows:

1. **Strong Event:** Peak abundances of IRD and *N. pachyderma (s)* occur within the same sample interval (IRD abundance ≥ 5.0%, *N. pachyderma (s)* ≥ 10.0%)
2. **Weak Event:** Peak abundance of IRD, if present, does not occur within the same sample interval as peak *N. pachyderma (s)* abundance or significant IRD is not present (≥ 4.0%)
3. **Offset Event:** Significant peak abundances in IRD (≥ 4.0%) and/or *N. pachyderma* (≥ 10.0%) occur within < 3,000 years of each other and appear to correlate
4. **IRD:** significant (≥ 4.0%): (strong (≥ 5.0%), weak (4-5.0%)
5. **IRD:** insignificant (< 4.0%)

i. Strong IRD Signals: Heinrich 1 (~17,000) and Heinrich 4 (~37,000)

Heinrich Events 1- and 4-mark significant increases in ice-rafted debris at Site U1313. H1 has more variability in its IRD pattern, whereas H4 is a more discrete peak (Figure 9). H1's interval lasted 3.43 kyrs and H4's interval lasted 5.71 kyrs, suggesting that these events lasted for different durations at Site U1313. Both events were similar in signal strength, although H1 left a stronger IRD record than H4. Between H4 (~37,000) and H1 (~17,000), no significant increases in IRD (≥ 4.0%) were observed at Site U1313.

Heinrich Event 1 reaches its peak abundance of 10.03% at 17.1 kyrs (Figure 9). The increase in IRD leading up to H1 initiated around 18.3 kyrs within a larger warming, deglacial transition in the planktic *G. bulloides* $\delta^{18}O$ record. At this time, IRD increased from a low variability between 0.47% (21.7 kyrs) and 1.75% (18.9 kyrs) to 3.24% at 18.3 kyrs, 5.32% at 17.71, and then to peak abundance of 10.03% IRD at 17.1 kyrs (strong H1). The precursory variations in IRD before H1 correlate with a generally cool period in the planktic $\delta^{18}O$ record. H1 maintains a high IRD signal for approximately 1,000 years between 17.1 kyrs (10.03%) and 16.0 kyrs (9.09%) before declining significantly at 15.4 kyrs to a weaker IRD signal of 4.73%. Subsequently, this event is followed by two younger, smaller, and significant (≥ 4.0%) IRD peaks at 14.9 kyrs (8.56% IRD) and 13.1 kyrs (5.46%). All three of the most recent IRD signals occur within the warmest period of the planktic $\delta^{18}O$ record.

Heinrich Event 4 was another strong event for Site U1313. Though not as abundant as H1, H4 was second most abundant IRD signal within the 343 cm core section. At 37.1 kyrs, H4 increased to its peak abundance of 9.05% IRD (Figure 9). The

initial increase to this peak occurred around 44.0 kyrs, when IRD abundances grew from 0% between 48.6 and 46.0 kyrs to 2.01% IRD at 40.0kyrs. The increase reached a climax at 37.1 kyrs. H4's IRD is less well-resolved than H1 as it only has one data point to define its peak abundance, but this can provide a minimum estimate of the strength of the event. The relative abundance of IRD decreased rapidly after peak H4 conditions and declined to an insignificant level of 1.07% at 34.3 kyrs. H4's peak IRD signal directly correlates to a significant drop in temperature in the planktic $\delta_{18}O$ record. The *G. bulloides* record shows that a short warming trend followed H4.

ii. Weak IRD Signals: Heinrich 6 (~64-62,000) and Heinrich 7 (~75,000)

Heinrich Event 6 and 7 were less significant iceberg-discharge events compared to H1 and H4 (Figure 9). H6 (8.57 kyr interval) had a longer duration than H1 and H4 (3.43 and 5.71 kyrs, respectively), but a less intense impact on the IRD record at this location. H7 had the shortest interval with an estimated duration of 2.57 kyrs. H6 and H4 have similar data resolution in the record, whereas H7 is better resolved. Therefore, there seems to be more variation in the peak at H7 compared to the general IRD trend in the H6 interval. There is little change observed in the IRD relative abundance of the core between intervals H7 and H6 (Figure 9).

H6 had a slightly wider IRD base than H7 and reached the third most abundant IRD peak of core U1313 at 62.9 kyrs (4.83%). The growth to H6's peak abundance began at 66.3 kyrs (0.34%) and increased steadily to 2.36% at 64.3 kyrs, before it reached 4.83% IRD. After this steady growth, a rapid decline to low IRD by 56.6 kyrs (0.61%) followed the H6 interval. The small increase in IRD to 1.12% at 51.4 kyrs was the only

change in IRD recorded between H6 and H4. H6 occurred in a cooling trend within the planktic $\delta^{18}O$ record. The event was located at the end of an increasingly cold period as temperatures declined from warmer conditions around 86.0 kyrs ($\delta^{18}O$ 1.52‰) to some of the coldest temperatures (heaviest $\delta^{18}O$) recorded by the G. bulloides record (3.03‰ at 51.7 kyrs). Unlike the dramatic warming after H4, H6 was followed by a small warming trend before declining to the heaviest δ18O values.

H7 is slightly more resolved than H6 and H4, though not as well resolved as H1. H7 reached its peak IRD abundance at 75.1 kyrs (4.40%). There was a slightly longer period of growth to H7's peak abundance. This period has a lower resolution, but IRD began to increase from 0.00% at 86.9 kyrs to 3.44% at 75.7 kyrs. Based on the large difference in these relative abundances, it is inferred that IRD increased closer to the 75 kyr transition mark. The variation after H7's peak abundance shows another rapid decline in IRD to a post-event low of 0.77% by 72.9 kyrs. Unlike H6 and H4, H7 occurred after a cooling trend and within an overall warmer period. Temperatures declined after 86.0 kyrs to heavier δ18O values of 2.38‰ at 78.0 kyrs. Then, the planktic record rose to warmer temperatures and lighter δ18O values of 1.99‰ at 75.7 kyrs. The warmest part of this overall trend correlates closely with the peak IRD abundance of H7. H7's IRD abundance decreased as the cooling trend resumed after 75.7 kyrs.

iii. Insignificant IRD Signals (≤4.00%): Heinrich 2 and Heinrich 5

A brief analysis of Heinrich Event 2 and 5 are included here to state that although the IRD abundances of these events did not reach the designated threshold of IRD significance, small IRD signals corresponded to correlated intervals of significant (≥

10.0%) increases in polar species *N. pachyderma (s)* (Figure 10). Therefore, the approximated timing of these events seen later in the results (Figure 10, 11, 12) is based on the presence of *N. pachyderma (s)* as an indicator of polar-like water and not the strength of the IRD signals (which is the basis for the timing of H1, H4, H6, and H7).

The Heinrich Event 2 interval is estimated during the small increase in IRD to 1.29% at 22.9 kyrs. This correlates to a significant increase in *N. pachyderma (s)* tat the same time (Figure 10). H2 also corresponds to low planktonic δ18O values indicative of the Last Glacial Maximum. The small IRD signal from Heinrich Event 5 is offset from the significant increase in *N. pachyderma (s)*. *N. pachyderma (s)* peaked at 54.0 kyrs, and IRD lagged in its increase to 1.12% IRD at 51.4 kyrs.

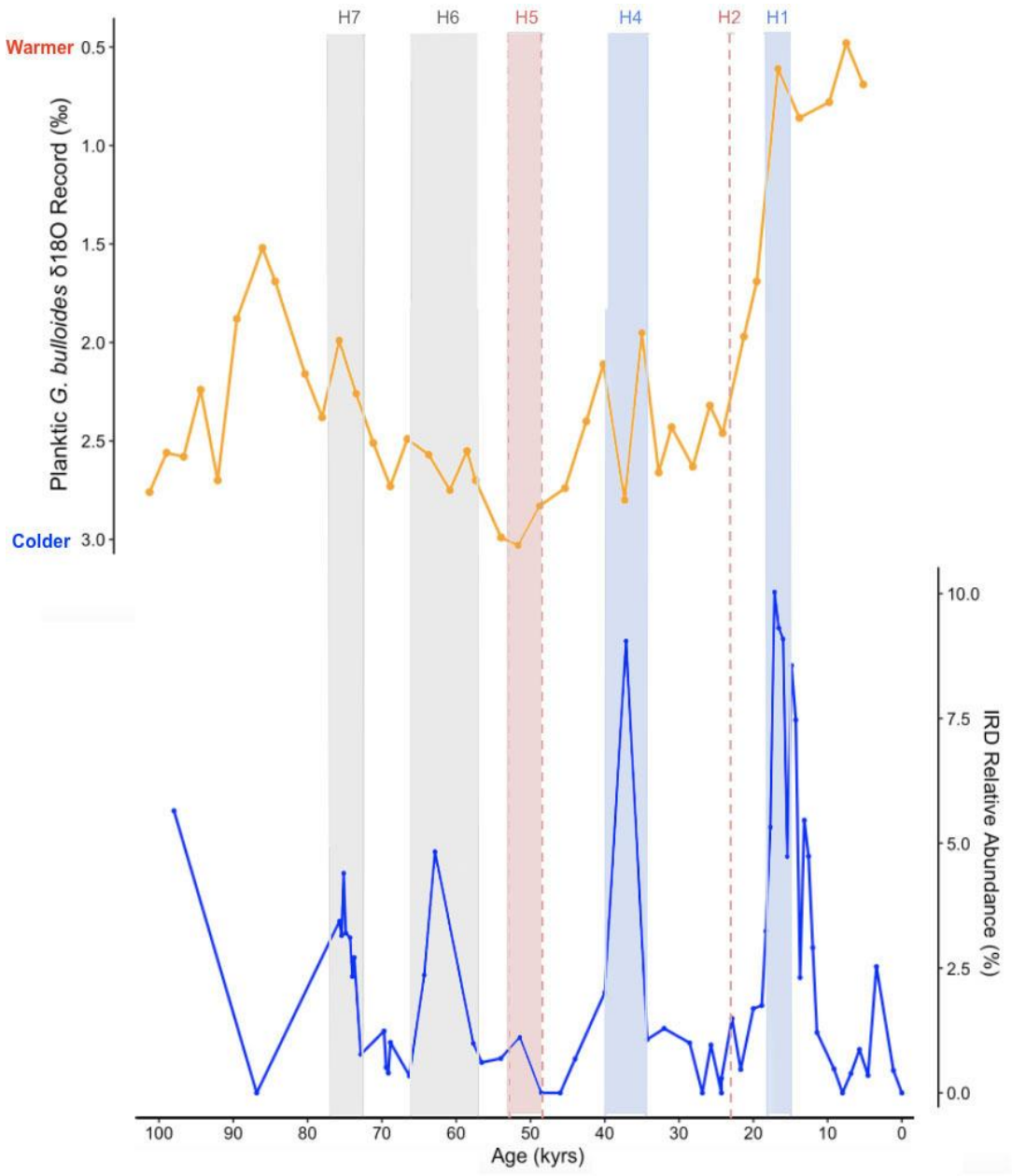

Figure 9. Comparison of the total percent of ice-rafted debris (IRD) grains in core U1313's coarse fraction (blue) to the $\delta^{18}O$ record of planktic foraminifera species *G. bulloides* (orange). Percent relative abundance is on the primary y-axis (right) and the planktic $\delta^{18}O$ record is on the secondary y-axis (left). Uncertainty calculations for percent relative abundance are in the Appendix (N). Indications of "warmer" and "colder" on the secondary y-axis indicate general changes in the surface ocean as a proxy for global climate trends (Kipp, 1976).

B. Relative Abundance of Temperature-Dependent Foraminifera Species

The relative abundances of three foraminifera species were recorded for the past ~100,000 years. Subsurface polar planktonic foraminifera species *N. pachyderma (s)* was plotted

against both the relative abundance of ice-rafted debris (Figure 10) and surface-dwelling subpolar species *T. quinqueloba* (Figure 11). Lastly, *N. pachyderma* was plotted against the subpolar/subtropical (transitional) and subsurface species *G. inflata.* The comparison of relative abundances of IRD and *N. pachyderma (s)* was used to build on the IRD analysis from the above section; the potential alignment of Heinrich Events 5 and 2 were based on trends in the *N. pachyderma (s)* and literature ages for both Site U1313 and other North Atlantic sites (Naafs et al., 2013; Hemming 2004).

Important to note when comparing to the results from the above IRD section is that the primary y-axis for the following graphs increased to 20% for *N. pachyderma* and *T. quinqueloba* analyses and 25% for *G. inflata.* IRD reached lower overall abundances than the three individual foraminifera species and its pattern appears smaller than before (Figure 10).

i. Ice-Rafted Debris and Subsurface Polar Foraminifera Species

The variation in the relative abundances of both IRD and *N. pachyderma (s)* grain species significantly correlated ($R^2 = 0.67$; Appendix O). Previously identified Heinrich events H1, H4, H6, and H7 (Figure 9) are all supported by strong increases in the relative abundance of *N. pachyderma (s)*(Figure 10). Anomalously colder periods not supported by increases in IRD are noted in the *N. pachyderma (s)* record. In comparison with the Heinrich event literature ages, these periods may be evidence of the climatic signal of H5 and H2 at Site U1313 (Naafs et al., 2013; Hemming 2004; Broecker et al., 1992).

In addition to reaching the most abundant IRD values, Heinrich Event 1 also reached the most abundant *N. pachyderma (s)* levels (Figure 10). H1 is classified as a strong event as it reached its peak *N. pachyderma (s)* abundance of 21.59% and its peak

IRD abundance (10.03%) at the same time (17.1 kyrs)(Figure 9; Figure 10). The increase in *N. pachyderma (s)* at Site U1313 initiated between 21.7 kyrs (2.37%) and 20.0 kyrs (12.3%) and aligned with the deglacial transition out of the Last Glacial Maximum (Pflaumann et al., 2003; Lisiecki & Raymo, 2005). The growth of *N. pachyderma (s)* eventually culminated at 17.1 kyrs ,near the end of the warming period, and then had a saw-toothed decline as it approached the Holocene and reached its lowest values of 0.4% at 4.6 kyrs. The variation in the *N. pachyderma (s)* relative abundances relates closely with the observed changes in IRD during H1.

A weak potential alignment is proposed for Heinrich Event 2 (Figure 10). There is no observed significant peak in IRD abundance, but there is a significant increase in the abundance of *N. pachyderma (s)* at 22.9 kyrs to 10.9% (1.49% IRD). This increase corresponds to the very cold period in the *G. bulloides* record right before the deglacial transition and H1 event. A smaller peak of 4.5% *N. pachyderma (s)* at 26.9 kyrs preceded this increase.

Despite H4 reaching a similar peak IRD abundance as H1, the event had threshold *N. pachyderma (s)* abundances (10.0%). H4 is classified as a strong event as it reached its greatest *N. pachyderma (s)* value at the same time as its peak IRD abundance, like H1. The H4 event had its highest level of the polar species at 37.1 kyrs (10.0%). However, this is less than half the polar species abundance of H1 (21.6%). The peak corresponds to a cold period in the δ^{18}O planktic record, and the *N. pachyderma (s)* abundance declines simultaneously with the warming trend after H4.

Like H2, the proposed estimate for Heinrich Event 5 was based solely on the signal observed in the *N. pachyderma (s)* record. The period of increased *N. pachyderma*

(s) was slightly longer (8 kyrs) than H2 (discrete point) and was marked with interval bars instead of a dashed line (Figure 10). *N. pachyderma (s)* rose from 11.3% at 57.7 kyrs to its peak of 15.9% at 54.0 kyrs. The growth in the relative abundance of *N. pachyderma (s)* preceded a small increase in IRD at 51.4 kyrs to 1.12% (both included in the indicated H5 interval). These changes are located within the planktic record's coldest δ^{18}O values.

Peak IRD and *N. pachyderma (s)* abundances are more closely correlated for Heinrich Event 6 (1.63 kyr offset) than H5 (2.57 kyr offset), but H6 was a weaker amplitude than either H1 or H4. Within the proposed time interval for H6, peak *N. pachyderma (s)* abundance occurred at 64.3 kyrs (15.0%), which is offset from its later peak in IRD at 62.9 kyrs (4.83%) (weak and offset signal). There was a rapid increase in the polar species starting at 66.3 kyrs (4.8%) before it reached its peak abundance shortly after. The H6 interval correlates to a relatively cold period that did not experience as much variation in the δ^{18}O record as H1 or H4. Compared to the steep decline in *N. pachyderma (s)* observed after H1, the polar species maintained a relatively abundant profile at Site U1313 after the H6 interval before leading into H5.

H7 has an interesting *N. pachyderma (s)* profile. The IRD and polar foram grain species vary together as closely as the H1 interval (Figure 9; Figure 10). H7 reached its peak *N. pachyderma (s)* abundance at the same time as its peak IRD, but it is not classified as a strong event as it did not surpass ≥ 5.0% IRD. At 75.1 kyrs, the peak relative abundance of *N. pachyderma (s)* was 13.7% and 4.40% IRD. These values occurred after a brief warming within the general cooling trend between 86.6 kyrs (1.52‰ δ^{18}O) and 51.7 kyrs (3.03‰ δ^{18}O). The polar species declined quickly after its peak abundance, and the δ^{18}O record began to cool again. There was another increase in

N. pachyderma (s) between the estimated time intervals for H7 and H6 at 69.7 kyrs (12.0%), but there were no observed changes in the relative abundance of IRD.

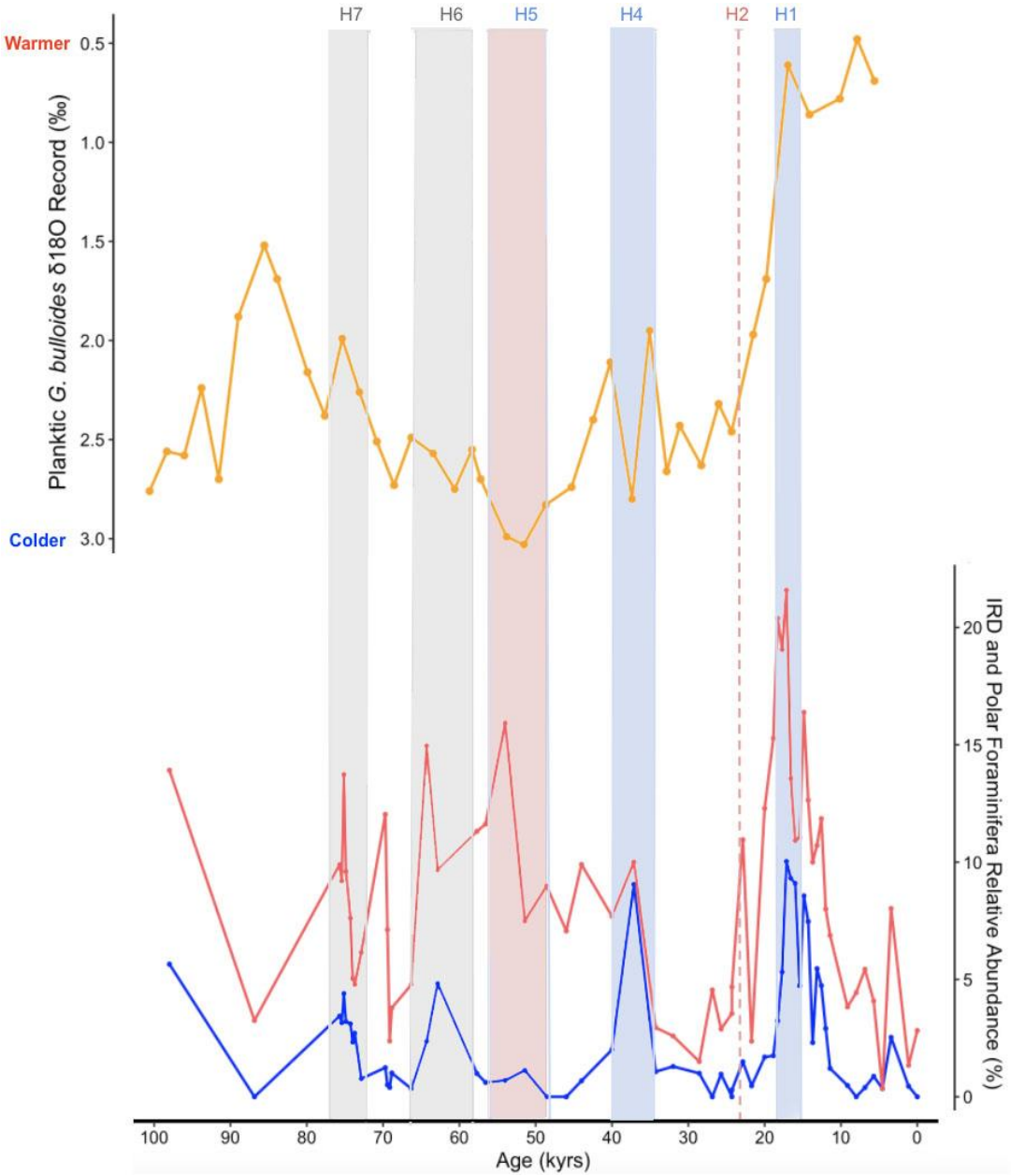

Figure 10. Relationship between the percent relative abundance of ice-rafted debris (IRD) (blue) and *N. pachyderma (s)*(red) plotted against the δ^{18}O planktic record (orange) of core U1313. Primary axis shows the grain species as a percentage of the total coarse fraction (right) and secondary axis relates to the δ^{18}O *G. bulloides* record (left).

ii. Polar (subsurface) and Subpolar (surface) Foraminifera Species

Subpolar species *T. quinqueloba* maintained an average relative abundance of 5.99% between 18.3 and 14.9 kyrs during the recent periods of this core (Figure 11). The average *T. quinqueloba* abundance was steady during the deglacial trend in the planktic δ^{18}O record. *T. quinqueloba* was 4.6% of the coarse fraction at H1's peak IRD and *N. pachyderma (s)* abundances of 17.1 kyrs. *T. quinqueloba* reached its peak abundance slightly later, around 16.6 kyrs (7.2%). The first significant decline in *T. quinqueloba* occurred after H1 at 12.6 kyrs. It dropped to a relative abundance of 2.8%, close to the warmest temperatures of the planktic δ^{18}O record.

There was no significant change in the *T. quinqueloba* record for Site U1313 near the proposed timing of H2. A small increase in the subpolar species from 0.7% to 3.5% occurred between 24.3 – 22.9 kyrs, but this appears to be one of lowest relative abundances of *T. quinqueloba* in the core. During the deglacial transition, *T. quinqueloba* abundance decreased around 18.9 kyrs to 1.3% before climbing to its more abundant H1 profile.

H4 appears to have an offset *T. quinqueloba* and *N. pachyderma (s)* signal. H4 has its peak *T. quinqueloba* abundance older in its interval at 40.0 kyrs (12.4%), preceding the peak *N. pachyderma* abundance at 37.1 kyrs (10.0%). This is also the most abundant *T. quinqueloba* interval throughout core U1313. During peak *N. pachyderma (s)* abundance, *T. quinqueloba* was declining until it reached a low abundance at 32.0 kyrs (0.9%). During the H4 interval, *T. quinqueloba* levels steadily declined despite both a cooling and warming trend in the planktic δ^{18}O record.

T. quinqueloba and *N. pachyderma (s)*varied inversely within the estimated H5 interval. At 54.0 kyrs, *N. pachyderma (s)* was 15.9% of the coarse fraction whereas *T. quinqueloba* was only 1.4% of the total sample. The low *T. quinqueloba* values correlate with the coldest interval in the δ^{18}O record. However, *T. quinqueloba* increased soon after to 9.4% and *N. pachyderma (s)* decreased from its peak abundance to a lower average value of 9.0% (48.6 kyrs). The increase in *T. quinqueloba* and decrease in *N. pachyderma (s)* is correlated with a warming trend in the planktic δ^{18}O record.

The two foraminifera species also vary inversely during the H6 interval. During peak *N. pachyderma (s)* abundance (15.0% at 64.3 kyrs), *T. quinqueloba* was only 4.7% of the coarse fraction. There was a small increase in *T. quinqueloba* at 62.9 kyrs to 7.2% and accompanied decrease in *N. pachyderma (s)* to 9.7%. The planktic δ^{18}O record for H6 did vary as drastically as other Heinrich intervals, but the coldest part of the period lead to an increase in *N. pachyderma (s)* and decrease in *T. quinqueloba* that precede the H5 interval.

T. quinqueloba and *N. pachyderma (s)* covaried during the H7 interval. However, peak *T. quinqueloba* abundance preceded peak *N. pachyderma (s) abundance* by a small amount. *T. quinqueloba* was most abundant at 75.4 kyrs (7.3%). The species then declined to 4.9% when *N. pachyderma (s)* reached its peak abundance at 75.1 kyrs (13.7%). Both peak abundances for these species occur within the cooling trend that occurred after the warmer δ^{18}O values of 75.7 kyrs (1.99‰). There was a similar increase in *T. quinqueloba* at 69.7 kyrs (between proposed H7 and H6 intervals) to 9.1% of the coarse fraction which was reflected in the earlier *N. pachyderma (s)* record. The peak correlates with a cold period in the planktic δ^{18}O record.

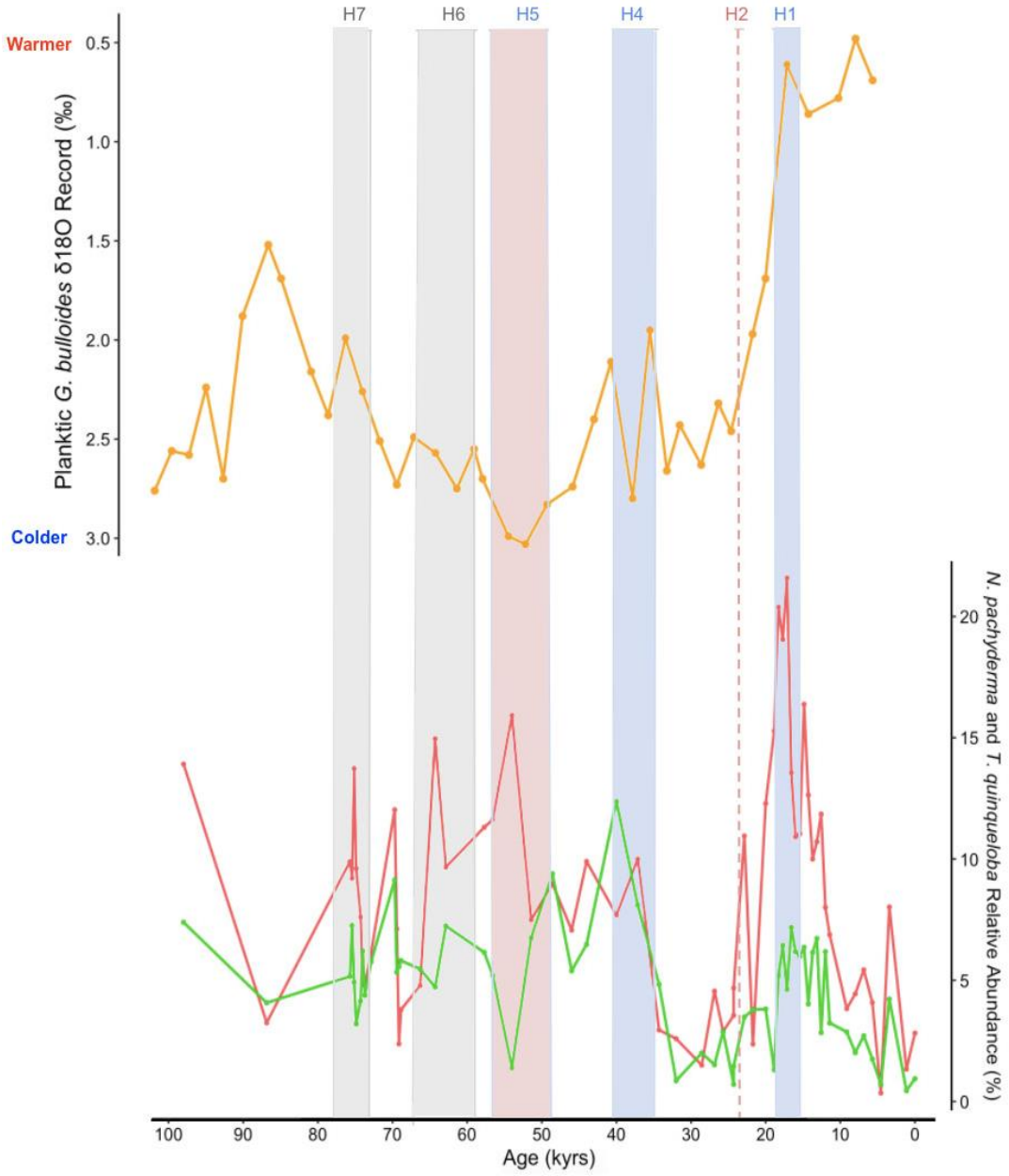

Figure 11. Variation in the percent relative abundance of polar planktonic foraminifera species *N. pachyderma (s)* (red) and subpolar planktonic foraminifera species *T. quinqueloba* (green) in core U1313's coarse fraction. Primary y-axis shows the percent of both foraminifera species (right) and the secondary y-axis represents the planktic δ^{18}O record of *G. bulloides* (left).

iii. Polar and Transitional Subsurface Foraminifera Species

G. inflata varied inversely with *N. pachyderma (s)* during the H1 interval (Figure 12). As *N. pachyderma (s)* rose to its most abundant level, *G. inflata* declined rapidly from 16.6% at 21.7 kyrs to 4.4% at 17.1 (peak IRD and *N. pachyderma (s)* abundances).

After the peak of H1, *N. pachyderma (s)* began to decline and *G. inflata* increased to a steady average abundance of 8.34% until 8.0 kyrs B.P. The general decline in the relative abundance of *G. inflata* fell within the deglacial transition towards warmer Holocene conditions.

The proposed alignment of H2 occurred at the end of a dramatic change in both *G. inflata* and *N. pachyderma (s)* abundances. *G. inflata* was the most abundant foraminifera species throughout the core between the H4 and H2 intervals. At 26.9 kyrs, *G. inflata* was 25.8% of the coarse fraction. *N. pachyderma (s)* was a small amount of the coarse fraction during this interval (4.5%) and no IRD was recorded. After this peak abundance, *G. inflata* decreased until it reached 11.4% at peak *N. pachyderma (s)* abundance for this interval at 22.9 kyrs (10.9%). *G. inflata* briefly increased at the start of the deglacial transition to 16.6% (21.7 kyrs) and then declined to lower abundances.

H4 had relatively equal levels of *N. pachyderma (s)* and *G. inflata.* At 40.0 kyrs, the two foraminifera species were almost equally abundant. *N. pachyderma (s)* was 7.7% of the coarse fraction and *G. inflata* was only slightly more dominant (8.0%). Then, *N. pachyderma (s)* rose quickly to 10.0% and *G. inflata* rose to 8.6% at 37.1 kyrs. Within the cold period after H4, *G. inflata* grew steadily to its peak abundance at 26.9 kyrs and *N. pachyderma (s)* had a minor presence.

Unlike the other events, *G. inflata* and *N. pachyderma (s)* varied similarly throughout the proposed H5 interval. *N. pachyderma (s)* was more abundant than *G. inflata* during this period, and *G. inflata* only reached a peak abundance of 5.9% at 54.0 kyrs. At the end of this interval, *G. inflata* increased from a low abundance (3.4% at 51.4 kyrs) to 10.1% at 46.0 kyrs in relation to a warming trend in the planktic $\delta^{18}O$ record.

There were no dramatic changes in the relative abundance of *G. inflata* during H6. The species reached a peak abundance of 7.1% at 64.3 kyrs but declined for the remainder of the interval (low of 4.4% at 57.7 kyrs). The decrease in *G. inflata* was inversely related to *N. pachyderma (s)*, which increase towards the end of the event period. The H6 trend fell within a brief cooling period in the *G. bulloides* δ^{18}O record.

G. inflata reached one of its lowest abundances in core U1313 in the H7 interval at peak IRD and *N. pachyderma (s)* abundances. At 75.1 kyrs, *G. inflata* was only 1.8% of the coarse fraction. Right before the peak abundance of these two proxies, *G. inflata* increased from 1.7% (75.7 kyrs) to 6.5% (75.4 kyrs). It then declined to a steady low abundance. This small increase relates to a warming in the planktic δ^{18}O record and slightly precedes the increase in *N. pachyderma (s)* and IRD of H7. As H7 terminated, *G. inflata* rose to comprise 11.7 % of the coarse fraction at 69.4 kyrs, even though the δ^{18}O record was cooling.

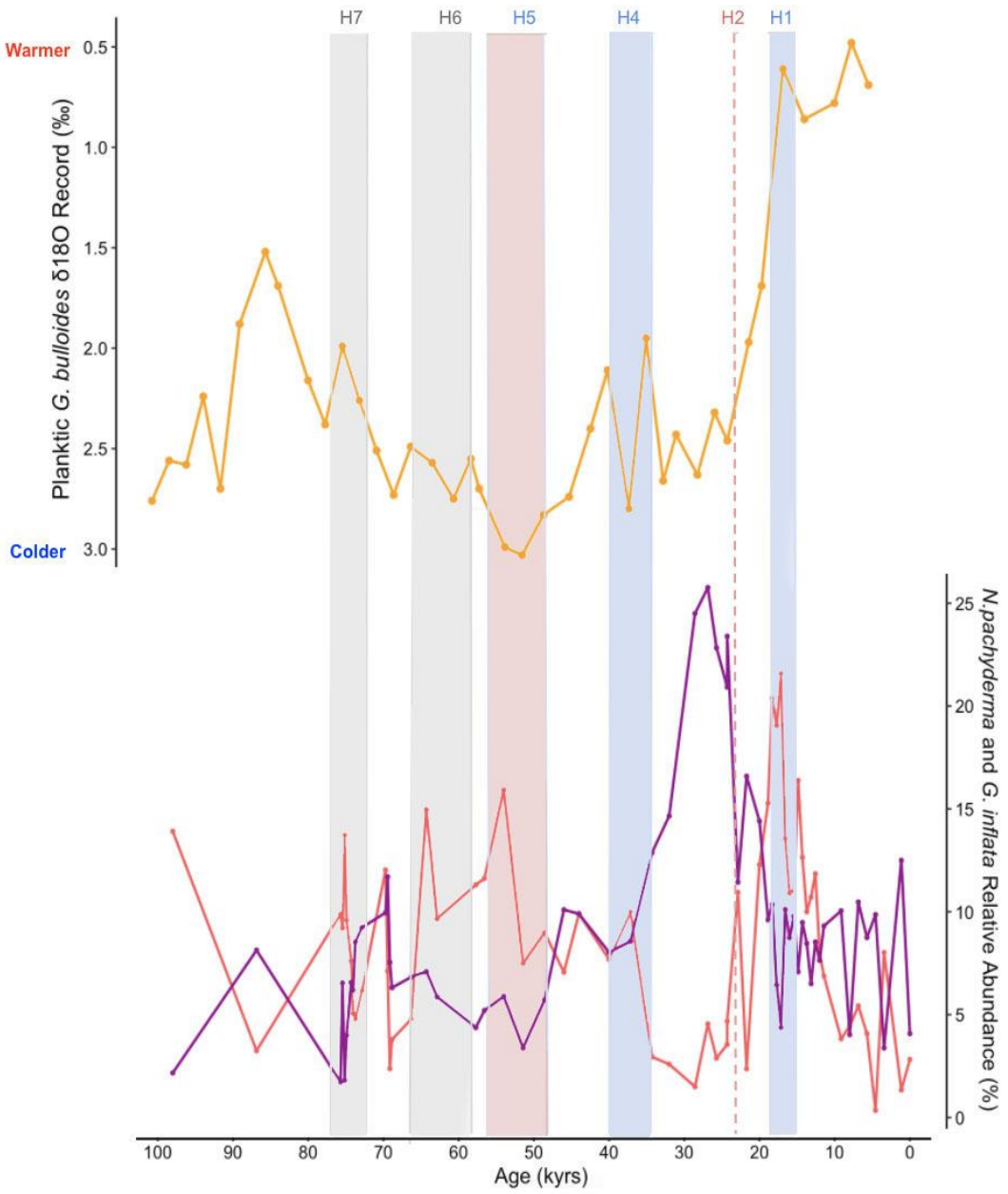

Figure 12. Abundance of polar planktonic foraminifera species *N. pachyderma (s)* (red) and subpolar/subtropical planktonic foraminifera *G. inflata* (purple) compared to the planktic δ^{18}O record of *G. bulloides* (orange). Primary y-axis shows the percent of both foraminifera species (right) and the planktic δ^{18}O record of *G. bulloides* is on the secondary y-axis (left).

C. Summary of Estimated Age Alignments for Heinrich Events

The estimated ages of Heinrich Events 1, 2, 4, 5, 6, and 7 (RDT) are based on the observed signal strength between the ice-rafted debris and *N. pachyderma (s)* relative abundance records (Table 1). Heinrich Events 1 and 4 had the strongest correlation between peak

IRD and *N. pachyderma (s)* abundances. Heinrich Events 6 and 7 were weak signals but reached significant levels of both IRD and *N. pachyderma (s)*. Heinrich Events 2 and 5 were insigifniciant IRD signals and were dated based on strong increases in the *N. pachyderma (s)* record. Heinrich Events 5 and 6 were labeled as offset and given a wider potential time interval as their peak IRD and *N. pachyderma (s)* abundances exhibited a lead-lag pattern (< 3 kyrs). Additionally, potential sources of ice-rafted detritus were included based on the literature classification of H1, H2, H4, and H5 as "Hudson Strait" events (Hemming, 2004). H6 and H7 are not exclusively related to iceberg-discharge from the Laurentide Ice Sheet.

Table 1. Summary table of the estimated age alignment of Hudson Strait (HS) Heinrich Events 1, 2, 4, 5, and non-Hudson Strait Heinrich Event 6 in Core U1313. Proposed change in the North Atlantic Ocean's major iceberg-discharge depositional axis was also estimated (Ruddiman, 1977b). Event signal strength was based on the observed percent abundance of IRD (strong ≥ 5%, weak 4-5%) and correlated signal response of *N. pachyderma (s).*

Heinrich Event	U1313 Age Alignment (kyr)	Literature Age (kyr)	Potential IRD Source	Signal Strength	IRD Abundance (%)	*N. pachyderma* Abundance (%)	*T. quinqueloba* Abundance (%)	*G. inflata* Abundance (%)
H1	17.1	17.4° || 16.8*	HS	strong	**10.03**	**21.59**	4.63	4.37
H2	~ 22.9	24.5 || 24	HS	weak	1.49	10.95	3.48	11.44
H4	37.1	39 || 38	HS	strong	9.05	10.00	8.10	8.57
H5	54.0 – 51.4	49 || 45	HS	offset/weak	0.69 – 1.12	15.92 – 7.49	1.39 – 6.74	5.88 – 3.37
H6	64.3 – 62.9	60 || 60	non-HS	offset/weak	2.36 – 4.83	14.96 – 9.66	4.72 – 7.24	7.09 – 5.86
H7/RDT	~ 75.14	75†	non-HS	weak	4.40	13.76	4.92	1.81

°Naafs et al. (2013; Site U1313) || *Hemming (2004), †Ruddiman (1977a, 1977b)

IV. DISCUSSION

Iceberg-discharge events have been identified within the IRD belt, but variations in sea surface temperature (SST), surface ocean circulation, and water mass migration outside of this region is less well-understood (Heinrich, 1988; Bond et al., 1992; Hemming, 2004). Site U1313's position outside the southern boundary of the IRD belt can better resolve our understanding of the dominant climatic and oceanic circulation patterns in the subpolar-subtropical region as this sedimentary record most likely reflects more extreme iceberg-

discharge events (Figure 8; Ruddiman,1977a;). Most core sediment coverage is restricted to the central IRD belt; it is crucial we look beyond this region to build a complete picture of the North Atlantic's oceanographic profile in glacial times. Core U1313 provides new evidence on the strength and impacts of cyclic iceberg-discharge events on the central North Atlantic Ocean for the past glacial cycle (Naafs et al., 2013).

The discussion on Heinrich Events from the last glaciation has focused on identifying six major events throughout the last ~60 kyrs (Heinrich, 1988; Bond et al., 1992; Broecker et al., 1993). Therefore, this analysis is divided into three sections. The first will discuss the estimated age alignments for Heinrich Events 1, 2, 4, 5, and 6 in Site U1313's sedimentary record and comparison with core data closer to the IRD belt. The second will address Site U1313's potential climatic and oceanic response to these events. The final section will consider the impacts of the major ice-rafted debris depositional transition at 75,000 on Site U1313 and the North Atlantic's circulation (Ruddiman, 1977a, 1977b).

A. Alignment of Heinrich Events in Core U1313 for the Past ~60,000 years

i. Strong & Synchronous IRD Signals: Hudson Strait (HS) H1 and H4

Hudson Strait Heinrich Events 1 and 4 were intervals of strong IRD and *N. pachyderma (s)* signals in core U1313 and other sites throughout the North Atlantic Ocean (Hemming, 2004; Naafs et al., 2011). In other sediment cores, the coarse fraction of these Heinrich layers is particularly dominated by Paleozoic carbonates, whose main provenance in the circum-Atlantic region is from the Hudson Strait (Appendix Q; Gwiazda et al., 1996; Hemming, 2004; Naafs et al., 2011). Heinrich Event 1 is linked to a great destabilization of the Laurentide Ice Sheet (LIS) and is commonly one of the most

dramatic iceberg-discharge events recorded in North Atlantic sedimentary records (Bond et al., 1992; MacAyeal, 1993; Bond & Lotti, 1995). Heinrich Events 1, 2, 4, and 5 have all been proposed as LIS-based events, which makes the discriminate H1 and H4 signal in core U1313 more interesting.

Site U1313 experienced the greatest total IRD deposition during the estimated HS-H1 interval (Figure 9). The significant and nearly simultaneous increase in polar species *N. pachyderma (s)* and ice-rafted debris nearly ~17,000 years ago suggests that Site U1313 was impacted by the circulatory IRD and oceanic temperature pattern associated with this event. The age alignment for Heinrich Event 1 was based on the relative timing of the two sedimentary proxies' peak abundances. In HS-H1's case, the interval with the sharpest increase in IRD at 17.1 kyrs (10.03%) also had the strongest peak in *N. pachyderma (s)* (21.59%; Figure 9). The estimated timing for HS-H1 aligns with previous age estimates that ranged between 17-17.5 kyrs (Table 1)(Hemming, 2004; Heinrich, 1988; Naafs et al., 2013; Hodell et al., 2017). More northern cores have given HS-H1 slightly older ages, suggesting that Site U1313 felt the effects of this event after icebergs circulated through the subpolar North Atlantic (Álvarez-Solas et al., 2011). The upper section of the core is highly resolved and precise variations in the iceberg-discharge cycling of HS-H1 are recorded (Figure 9).

Additionally, these results support previous research that posited Heinrich Event 1 as a two-stage event. The first peak, H1.1., was estimated for Site U1308/DSDP 609 (49°53' N, 24°14'W) to have potentially occurred at ~16.2 kyrs (15.5-17.1) and H1.2 at 15.1 kyrs (14.3-15.9)(Bond et al., 1992; Sancetta, 1992; Hodell et al. 2017; Stanley, 2017). Site U1313's most abundant IRD peak was at 17.1 kyrs, and two smaller peaks in

IRD followed at 16.0 kyrs (9.09%, as strong as HS-H4) and 14.9 kyrs (8.56%). The HS-H1 peak is well-defined across cores (Hemming, 2004). The two younger peaks are potentially indicative of H1.2 or even a small third sub-event in core U1313 (Hodell et al. 2017).

HS-H4 was the second most abundant IRD event at site U1313 (Figure 9). Like H1, it reached simultaneous peak *N. pachyderma (s)* and IRD abundances. At 37.1 kyrs, *N. pachyderma (s)* was 10.0% and IRD was 9.04% of the coarse fraction. The literature age for this event has been estimated at approximately ~37-35,500 years and supports the identification of these peak abundances in core U1313 as HS-H4 (Table 1)(Bond et al., 1992; Hemming, 2004). HS-H4 is known for its creation of powerful iceberg armadas across the North Atlantic, but it was not the strongest IRD signal at Site U1313 (Broecker et al., 1992; Hemming, 2004). This could be because Site U1313 was too far south to experience the high-level of IRD deposition associated with event. However, the presence of 9.04% IRD suggests that icebergs did reach this site, potentially before they circulated to more northeasterly sites. At cores VEMA 28-82 (49°45'N, 22°27'W) and DSDP 609, slightly northeast of this site and well-within the IRD belt, HS-H4 is estimated to be more recent (~34,000, ~35,000) than the Hs-H4 layer in core U1313 (~37,000). These icebergs likely were able to travel farther south in the subpolar cyclonic gyre before reaching the more northeasterly sites, or early iceberg-discharge from HS-H4 headed towards this site before more icebergs were released towards the north-central regions (McManus et al. 1998, Bond et al., 1993, Bond et al., 1999). HS-H4 IRD is recorded at Site U1313 before core VEMA 23-81 (54°25'N, 16°83'W, even further northeast than V28-82 or DSDP 609) which similarly estimates HS- H4 around ~35,500

kyrs (Bond et al., 1993; Hemming, 2004). Lack of an IRD signal at more northeasterly cores while IRD is observed at Site U1313 argues that this iceberg-discharge event originated from the Hudson Strait and its icebergs flowed in a cyclonic pattern in the North Atlantic's subpolar gyre (Appendix A; Ruddiman, 1977a; Heinrich, 1988)). At Site SU 90-08 (43°50N, 30°40W, closer but still slightly NE of Site U1313), HS-H4 was also dated to approximately ~35,000 years (Zahn et al., 1997; Cortijo et al., 1997). Therefore, some caution is required when comparing the timing of HS-H4 in core U1313 to the larger North Atlantic region.

ii. Weak & Low-IRD Signals: Hudson Strait (HS) Heinrich Events 2 and 5

Similar signals might be expected from the remaining Hudson Strait Heinrich Events 2 and 5 based on the strong IRD and *N. pachyderma (s)* signals from HS-H1 and HS-H4. Contrastingly, there were no significant peaks in IRD (≥4.0%) for the estimated HS-H2 and HS-H5 intervals (Figure 9). In other cores, HS-H2 and HS-H5 are identified by their unmistakable increases in IRD within the coarse fraction and estimated to have occurred around 24.5-21 kyrs and 45-50 kyrs, respectively (Bond et al., 1992; Bond et al., 1993; Hemming, 2004; Naafs et al., 2013).

Site U1313's sedimentary record for HS-H2 and HS-H5 was examined during these two periods. Only changes in the relative abundances of the foraminifera proxy species were observed (Figure 10, 11, 12). Despite the lack of IRD, a proposed age alignment for HS-H2 and HS-H5 was created for core U1313 to compare the climatic signal captured in the planktic foraminifera records to HS-data from other studies. Hemming (2004) and Naafs et al. (2013) proposed H2 may be between ~24 - 24.5 kyrs

but 0% IRD was found in core U1313 at 24.3 kyrs. Thus, the proposed age estimate for H2 (based only on the *N. pachyderma (s)* signal) should be applied to make surface-level comparisons and is not a suggestion to re-calculate the literature age(s) for H2. The same is true for HS-H5; the proposed age alignment for these events at Site U1313 is susceptible to change and would benefit from radiocarbon dating of the foraminifera in these levels.

HS-H2 was located at approximately 22.9 kyrs due to the significant increase in polar species *N. pachyderma (s)* at this time (10.9%; Figure 10). This estimate is aligned with the literature age interval for H2, despite the absence of a dramatic change in IRD at Site U1313 (Table 1). There was a small IRD increase at 22.9 kyrs to 1.29% of the coarse fraction and a small number of icebergs may have reached this site, but not nearly as many as during HS-H1 and HS-H4. The significant *N. pachyderma (s)* and absent IRD signal for the HS-H2 interval suggests that Site U1313 was more affected by changes in surface ocean circulation and temperature than the presence of a large iceberg armadas during this event. Other sites like DSDP 609 and V23-81 had relatively low overall foraminifera abundances for HS-H2 and were overrun by the presence of *N. pachyderma (s)*(Bond et al. 1992; Broecker et al., 1993). The variation in Site U1313's *N. pachyderma (s)* record may help resolve more subtle changes in surface ocean temperatures and circulation during HS-H2 (see Section B).

The peak abundance of *N. pachyderma (s)* lead the weak IRD signal of HS-H5. Polar species *N. pachyderma (s)* increased to 15.9% at 54.0 kyrs, slightly older than the literature ages (45-50 kyrs) for HS-H5 (Figure 10) (Hemming, 2004; Naafs et al., 2013). A small increase in IRD to 1.12% lagged the *N. pachyderma (s)* peak abundance at 51.4

kyrs, hinting that Site U1313 experienced a cooling in the surface ocean or subsurface waters before the arrival of icebergs. HS-H5 was the only Hudson Strait event that had an offset signal between its peak IRD and *N. pachyderma (s)* abundances at Site U1313, regardless of signal strength. Estimates from North Atlantic Site DSDP 609 place HS-H5 closer to 49-51 kyrs, which supports that the minor increase in IRD at 51.4 kyrs in this record may be evidence of icebergs from the LIS (Broecker et al., 1992; Hemming, 2004).

The change in IRD at 51.4% is closer to the literature age estimate for HS-H5, but the increase in *N. pachyderma (s)* precedes this signal. The proposed interval for HS-H5 in this study is a potential indicator of a precursory event recorded in the foraminiferal assemblage of Site U1313. Core U1313 recorded only small increases in IRD ≤ 1.5% for both HS-H2 and HS-H5, but its robust foraminifera record is informative on its own. The lead-and-lag signal within this interval suggests a wide-spread cooling pattern throughout the North Atlantic preceding the catastrophic release of icebergs during HS-H5 (reflected in the planktic δ^{18}O record between 86.0 and 51.7 kyrs).

iii. Weak & Offset IRD Signal: Heinrich Event 6

H6 is not as well understood, neither temporally nor spatially, as the powerful Hudson Strait Heinrich Events (Hemming, 2004). Research into recent Heinrich Events has compiled more data on the five younger events, leaving the impacts of H6 rather ambiguous (Broecker et al., 1992; Hemming, 2004). Despite this, studies have shown that H6 was a powerful iceberg-discharge event in the northeast North Atlantic and not linked to LIS instability (Heinrich 1988; Bond et al., 1992). H3 is also not classified as a

Hudson Strait Heinrich Event (H3 is not easily distinguishable within the IRD or *N. pachyderma (s)* records of most North Atlantic cores). These iceberg-discharge events probably originated due to instabilities in European rather than Laurentide icesheets (discharge through Norwegian and/or Irminger Sea pathways), or a combination of both (Ruddiman, 1977a; Bond & Lotti, 1995).

The current literature age for H6 is estimated to be about 66,000 years, though the uncertainty in this age may be up to 5,000 years (Meese et al., 1997 cited in Hemming, 2004). The alignment of this event at Site U1313 can constrain the timing for this event for the subpolar-subtropical central North Atlantic region (Heinrich, 1988; Bond et al., 1992). Unlike HS-H1 and HS-H4, H6 peak IRD and *N. pachyderma (s)* abundances were offset (Figure 10). The escalation in the relative abundance of *N. pachyderma (s)* preceded the growth in IRD, like HS-H5. The polar foram increased to 15.0% at 64.3 kyrs, slightly before IRD abundance grew to 4.83% of the coarse fraction at 66.3 kyrs. Again, this offset signal may be evidence of a regional SST climatic cooling before the presence of icebergs at Site U1313. The cold period preceding the H6 interval may be responsible for how European-based icebergs could survive melting long enough to circulate counterclockwise in the subpolar gyre to Site U1313 (Bond et al., 1992). Additionally, H6's peak IRD values (4.83%) were roughly half as abundant as HS-H1 and HS-H4 (10.03% and 9.05%). Over the past 60,000 years, Site U1313's temperature conditions were strongly impacted by HS-H1 and HS-H4 whereas the sedimentological signal from the weak, offset events HS-H5 and H6 are potential indicators of ocean-wide cooling. Site U1313 was not as heavily impacted by HS-H2 or HS-H5 despite these events sharing similar mechanisms and IRD provenance to HS-H1 and HS-H4.

B. Climatic and Oceanographic Impacts of Heinrich Events

The cyclic iceberg-discharge events of the past ~60,000 years have significantly impacted the climate and circulation of the central North Atlantic. The higher resolution of core U1313 (2 cm ≈ 571.4 years) has captured a regionally focused signal of the amplitude, extent, and possible migration of water masses and fronts related to Heinrich Event intervals. Only two of the more powerful Hudson Strait events, H1 and H4, were strongly present in both the IRD and *N. pachyderma (s)* core abundances. Heinrich Event 6 and 7 were classified as weak events, and H3 was not recorded at Site U1313, even though similar causation mechanisms are proposed for this event and H6 (Bond & Lotti, 1995; Hemming, 2004). H2 and H5 did not generate significant IRD records, but there was a significant cooling and increase in the polar and subpolar foraminiferal assemblages. These observations are useful tools for reconstructing potential changes in the surface ocean, water column, atmosphere, and ice-sheet dynamics of the glacial North Atlantic Ocean.

i. Ocean, Atmosphere, and Cryosphere Interactions

Heinrich Events are linked with the millennial-scale atmospheric variations observed over Greenland during the North Atlantic Ocean's past interglacial-glacial cycle (Bond & Lotti, 1995; Bond et al., 1993; Hemming, 2004). Different icesheet mechanisms have been proposed for the Hudson Strait-based events, but overall Heinrich Events are understood as the result of catastrophic iceberg-discharges due to instability in large icesheets surrounding the North Atlantic. Research into the correlation between Heinrich layers and shorter-scale climate variability in the air temperatures over Greenland (Dansgaard/Oeschger cycles) linked Heinrich events to generally cold periods that are

followed by brief but rapid warmings during the last glaciation (Bond et al., 1999; Bond & Lotti, 1995; McManus et al., 1996). These periods also correlate with wide-spread cooling in SSTs across the North Atlantic, though the amount and direction of temperature change at Site U1313 is under investigation (Heinrich 1988; Naafs et al., 2013).

A clear understanding of ice-sheet mechanisms related to Heinrich Events and their effect on the North Atlantic is still debated, but whether they are caused by a binge-purge or icesheet build-up and collapse mechanism, Heinrich events are often related to ice-sheet extent (Ruddiman, 1977a; MacAyeal 1993; Alley & MacAyeal, 1994). Ice-sheet growth and instability during both interstadial and stadial periods is the most likely cause to produce iceberg armadas in the North Atlantic Ocean (McManus et al., 1999; Hemming, 2004). Glacial periods have more variable global climates, which may be responsible for the rapid and distinct Heinrich layers across the polar and subpolar North Atlantic throughout the last glaciation.

One clear distinction between Heinrich events is their difference in IRD provenances. Extensive petrographic analysis of carbonate Heinrich layers has shown that H1, H2, H4, and H5 are mainly related to large instabilities and catastrophic iceberg-discharges from the Laurentide Ice Sheet into the Labrador Sea (Lehman & Keigwin, 1992; Broecker et al., 1992; Hemming, 2004). H6 and H3 are less well-constrained and may be the result of European-based ice sheets or a combination of circum-Atlantic iceberg sources. One proposed mechanism for both the southward shift in the major depositional IRD axis (H7) and other Heinrich Events is the migration and depression of the North Atlantic Drift current. Southward penetration of polar waters could decrease

the northward transport of heat by the NAC and cool northwestern Europe. On the other hand, this would also decrease the amount of moisture provided to the circum-Atlantic continental ice sheets (Ruddiman, 1977b). This mechanism is a complicated combination of both negative and positive feedback loops but mapping the subpolar-subtropical gyre boundary (north and south horizontal boundaries of the NAC) with sedimentary proxies places potential NAC migration within the context of Heinrich Events.

ii. Reconstructing Surface Ocean Circulation & Water Mass Distribution

Evidence of iceberg-deposition at Site U1313 is connected to a strengthening of the subpolar gyre, the southward penetration of polar waters into the central North Atlantic Ocean, migration of the North Atlantic Drift current and subtropical gyre shape, and/or alterations to the rate of Atlantic Meridional Overturning Circulation (Heinrich, 1988; Broecker et al., 1993; McManus et al., 1999). The midlatitude positioning of this core makes it a site-specific indicator of the effects of dramatic and abrupt climate change on the subtropical-subpolar ocean. However, the interpretations of the four sedimentary surface climate proxies included in this research most directly inform changes related to SSTs and shallow circulation.

The presence of IRD and increased abundances of cold-water foraminifera within the Heinrich layers in this record are strong indicators of a regional-scale shift in the water mass distribution of the central North Atlantic during iceberg-discharge intervals. These results agree with previous models that predicted Site U1313 may be included in the arctic front (8-20°C) during periods of extreme icesheet extent (CLIMAP, 1981; Pflaumann et al., 2003). Although Site U1313 experienced surface cooling during

Heinrich Events, it is unlikely it was covered by polar waters. The relative abundance of *N. pachyderma (s)* in polar waters is larger than 60%, and Site U1313's greatest peak in *N. pachyderma (s)* was only 21.59% (H1)(Figure 10; Ruddiman, 1977b). Therefore, polar waters did not directly cover Site U1313 for an extended period. Rather, the extension of the polar front likely caused a water-mass domino effect and pushed other surface waters southward. The expansion of the subpolar gyre would then explain the presence of abnormally cold SSTs at Site U1313. Seasonal variations in the strength and density gradients of the subpolar and subtropical gyre may have created a highly variable temperature environment at this site which is not discernable with the current time resolution of the core. Seasonal gyre control and age model variability are potential explanations for the inconsistency between this study's findings that Site U1313 was cooler during Heinrich Events and previous work that reported that opposite (Naafs et al., 2013).

The depth habitat relationship between subsurface species *N. pachyderma (s)* and surface-dwelling species *T. quinqueloba* reveals a comprehensive water column profile for the Heinrich event intervals (Figure 11; Bé & Tolderlund, 1971). *G. inflata* and *N. pachyderma (s)* compete within the same deeper habitat; variations between these species are reflective of drastically different and competing temperatures regimes in the water column (Figure 12). Therefore, *G. inflata* and *N. pachyderma (s)* tend to have an inverse relationship throughout this record (Figure 12). *T. quinqueloba* is generally less abundant than *N. pachyderma (s)* throughout the sediment record, though there are a few intervals where the subpolar species surpasses its polar counterpart. SSTs of overlying waters at Site U1313 for most of the last glaciation were cold and often a more favorable

temperature environment for *N. pachyderma (s)* than *T. quinqueloba* or *G. inflata.* On top of the generally cool climate of Site U1313 during Heinrich Events, HS-H1 and HS-H4 were particularly impactful events on the site's SSTs and water column stratification.

HS-H1 and HS-H4 both had high abundances of *N. pachyderma (s)* (21.59% and 10.0% respectively) and *T. quinqueloba* (4.63%, 8.10%) (Figure 10,11). Both HS-events also had low *G. inflata* abundances compared to modern assemblages (4.37% and 8.57%). The high concentration of *N. pachyderma (s),* medium concentration of *T. quinqueloba*, and low concentration of *G. inflata* during HS-H1 suggest that this was the coldest event at Site U1313. The medium amount of *N. pachyderma (s),* high abundance of *T. quinqueloba,* and medium abundance of *G. inflata* during HS-H4 indicates that this was a milder water column and SST environment compared to HS-H1 (Figure 11, 12). Together, these results support that Site U1313 was within the subpolar water regime during the strongest Heinrich Events (Pflauman et al., 2003).

The gyre distribution and SSTs of the central North Atlantic were less affected by HS-H2, HS-H5, H6, and H7. HS-H2 and H7 were classified as weak events (≤ 5.0% IRD) and respectively reached 10.95% and 13.76% *N. pachyderma (s),* 3.48% and 4.92% *T. quinqueloba,* and 11.44% and 1.81% *G. inflata.* The SST profile of HS-H2 was generally cold, but there was a more temperate water mass at depth. H7 was potentially one of the coldest periods at Site U1313 as it had a high percentage of both cold species and the lowest abundance of *G. inflata* throughout the entire record. HS-H5 and H6 were classified as weak/offset events as their peak abundances in *N. pachyderma (s)* occurred before the delivery of IRD (Figure 10, 11). HS-H5 reached 15.29% *N. pachyderma,* 6.74% *T. quinqueloba,* and 5.88% *G. inflata.* H6 had peak 14.96% *N. pachyderma (s),*

7.24% *T. quinqueloba*, and 7.09% *G. inflata* abundances. H6 and HS-H5 had similar peak *N. pachyderma (s)* and *T. quinqueloba* values, but the decrease in *G. inflata* from H6 to H5 suggests a cooling in the subsurface layer of the water column (supported by a low $\delta^{18}O$ values as well). Heinrich Events during this time were potentially responding to a cooling global climate and increased ice sheet growth. The sediment proxies from the weak and offset Heinrich Event layers showcase that iceberg delivery to the central North Atlantic is not the only potential mechanism responsible for regional cooling and that migration of the NAC is likely a relevant cause.

C. Transition of Ice-Rafted Debris Depositional Maximum at 75,000 B.P

i. Weak & Synchronous IRD Signal: Heinrich Event 7 (RDT)

The Ruddiman Depositional Transition event was a major shift at 75,000 B.P. in the dominant pattern of ice-rafting within the last interglacial-glacial cycle (Ruddiman, 1977a; 1977b). The major ice-melting axis (i.e. surface waters warm enough to melt passing icebergs) shifted southward from its interglacial positioning near Greenland and Newfoundland (MIS 5, 125-80 kyrs) to a band between 45°N-50°N, which it maintained for the last glacial cycle (Ruddiman, 1977a; 1977b). The relocation of the North Atlantic's depositional maximum was associated with water mass (polar front) migration, ice sheet growth and sea level decrease. Furthermore, this shift impacted the central North Atlantic Ocean and Site U1313's IRD and *N. pachyderma (s)* profiles (Figure 9, Figure 10).

The proposed timing of the RDT or Heinrich Event 7 in core U1313 aligns with the literature age for this interval (Ruddiman, 1977b). H7 was identified by the

simultaneous peak abundances in IRD (4.40%) and *N. pachyderma (s)* (13.7%) at 75.1 kyrs (Figure 10). H7 reached the fourth most abundant level of IRD in the core. In addition to the changes in sea level/ice storage on land during this period, the input of ice-rafted debris to the subpolar North Atlantic and the Norwegian Sea increased. The transport of icebergs to Site U1313 was most likely the same net cyclonic subpolar gyre circulation as predicted for the past six major Heinrich Events (Ruddiman, 1977a)

The southward penetration of colder waters and retreat of warmer waters in the North Atlantic Drift current allowed circum-Atlantic icebergs to travel farther in the subpolar gyre. Unlike the Hudson Strait Events, potential iceberg sources for this event may have come from both European (West Scandinavian, Barents), Greenland, or Laurentide ice sheets (Ruddiman, 1977a; 1977b; Hemming, 2004). H7 occurred in a warmer period within the early glacial period, and *N. pachyderma (s)* declined quickly after H7 (Figure 10). The abrupt transition in global climate is likely responsible for the extreme instability in icesheet growth and iceberg-discharge during H7. The relatively low IRD abundance of this interval may be because Site U1313 was in the subtropical gyre and many of the icebergs melted and dropped their IRD load before reaching the site. The North Atlantic maintained this depositional maximum for the remainder of the glacial period, and the six most recent Heinrich Events reflect this circulation in their IRD patterns.

V. CONCLUSION

The scale with which we investigate past climate variability predetermines the applicability of our conclusions. The limited spatial and temporal scope of this study was

intentionally chosen to generate a paleoclimate record possible of discussing sub-orbital, millennial scale changes in the North Atlantic Ocean's climate and circulation. The discovery of strong, weak, and offset Heinrich Event signals at IODP Site U1313 over the past 100,000 years posits the central North Atlantic Ocean as a relevant, informative, and potentially underutilized region in palaeoceanographic research. Site U1313's marine sediment record contains a nuanced yet concordant history of circulation changes in the North Atlantic during the last glacial period, despite its apparent midlatitude-isolation from major ocean, atmosphere, and cryosphere interactions. Moving forward, the inclusion of a benthic $\delta^{18}O$, $\delta^{13}C$, or radiocarbon record into this study's age model can decrease the current uncertainty surrounding the timing of Heinrich Events at Site U1313 and facilitate robust cross-site comparisons.

List of References

Alley, R.B. & MacAyeal, D.R. (1994). Ice-rafted debris associated with binge–purge oscillations of the Laurentide ice sheet. Paleoceanography 9, 503–511

Álvarez-Solas, J., Montoya, M., Ritz, C., Ramstein, G., Charbit, S., Dumas, C., Nisancioglu, K., Dokken, T., & Ganopolski, A. (2011). Heinrich event 1: An example of dynamical ice-sheet reaction to oceanic changes. *Climate of the Past*, *7*(4), 1297–1306. https://doi.org/10.5194/cp-7-1297-2011

Bé, A. W. H., & Hutson, W. H. (1977). Ecology of Planktonic Foraminifera and Biogeographic Patterns of Life and Fossil Assemblages in the Indian Ocean. *Micropaleontology*, *23*(4), 369–414. https://doi.org/10.2307/1485406

Bé, A.W. H., and Tolderlund, D.S. (1971). Distribution and ecology of living planktonic foraminifera in surface waters of the Atlantic and Indian Oceans. *Micropaleontology of Oceans*, edited by B. M. Funnell and W.R. Riedel, p. 105-149, United Kingdom: Cambridge University Press

Bolton, C. T., Wilson, P. A., Bailey, I., Friedrich, O., Beer, C. J., Becker, J., Baranwal, S., & Schiebel, R. (2010). Millennial-scale climate variability in the subpolar North Atlantic Ocean during the late Pliocene. *Paleoceanography*, *25*(4). https://doi.org/10.1029/2010PA001951

Bond, G., Broecker, W., Johnsen, S., McManus, J., Labeyrie, L., Jouzel, J., & Bonani, G. (1993). Correlations between climate records from North Atlantic sediments and Greenland ice. *Nature*, *365*(6442), 143–147. https://doi.org/10.1038/365143a0

Bond, G., Heinrich, H., Broecker, W., Labeyrie, L., McManus, J., Andrews, J., Huon, S., Jantschik, R., Clasen, S., Simet, C., Tedesco, K., Klas, M., Bonani, G., & Ivy, S. (1992). Evidence for massive discharges of icebergs into the North Atlantic ocean during the last glacial period. *Nature*, *360*(6401), 245–249. https://doi.org/10.1038/360245a0

Bond, G. C., & Lotti, R. (1995). Iceberg Discharges Into the North Atlantic on Millennial Time Scales During the Last Glaciation. *Science*, *267*(5200), 1005–1010.

Bond, G.C., Showers, W., Elliot, M., Evans, M., Lotti, R., Hajdas, I., Bonani, G., & S. Johnsen. (1999). The North Atlantic's 1-2 kyr climate rhythm: Relation to Heinrich events, Dansgaard/Oeschger cycles and the little ice age. *Mechanisms of Global Climate Change at Millennial Time Scales, Geophysical Monograph* 112, p. 35-68, edited by Clark, P. U, Webb, R.S., & L.D. Keigwin

Broecker, W. S. (1994). Massive iceberg discharges as triggers for global climate change. *Nature*, *372*(6505), 421–424. https://doi.org/10.1038/372421a0

Broecker, W., Bond, G., Klas, M., Clark, E., & McManus, J.F. (1992). Origin of the northern Atlantic's Heinrich events. *Climate Dynamics*, *6*, 265-273

Broecker, W., Bond, G., & McManus, J.F. (1993). Heinrich Events: Triggers of Ocean Circulation Change? In W. R. Peltier (Ed.), *Ice in the Climate System* (pp. 161–166). Springer. https://doi.org/10.1007/978-3-642-85016-5_10

Cenedese, C. & A.L. Gordon. (2011). Oceanic circulation [Image]. *Encyclopedia Britannica*, *https://www.britannica.com/science/ocean-current*

Channell, J.E.T., Kanamatsu, T., Sato, T., Stein, R., Alvarez Zarikian, C.A., Malone, M.J., and the Expedition 303/306 Scientists. (2006). *Proceedings of the Integrated Ocean Drilling Program, 303/306*. doi:10.2204/iodp.proc.303306.112.2006

CLIMAP Project Members (CLIMAP). (1981). Seasonal reconstructions of the Earth's surface at the Last Glacial Maximum. Map Chart Ser. MC-36. *Geological Society of America*, Boulder

Cortijo, E., Labeyrie, L., Vidal, L., Vautravers, M., Chapman, M., Duplessy, J.-C., Elliot, M., Arnold, M., Turon, J.-L., & Auffret, G. (1997). Changes in sea surface hydrology associated with Heinrich event 4 in the North Atlantic Ocean between 40° and 60°N. *Earth and Planetary Science Letters*, *146*(1), 29–45. https://doi.org/10.1016/S0012-821X(96)00217-8

Daniault, N., Mercier, H., Lherminier, P., Sarafanov, A., Falina, A., Zunino, P., Pérez, F. F., Ríos, A. F., Ferron, B., Huck, T., Thierry, V., & Gladyshev, S. (2016). The northern North Atlantic Ocean mean circulation in the early 21st century. *Progress in Oceanography*, *146*, 142–158. https://doi.org/10.1016/j.pocean.2016.06.007

eGeotraces Map Data. (2017). Potential Temperature of the North Atlantic Ocean. *eGEOTRACES Electronic Atlas*, https://www.egeotraces.org/sections/GA02_TPOT.html

Eynaud, F. (2011). Planktonic foraminifera in the Arctic: potentials and issues regarding modern and quaternary populations. *In IOP Conference Series: Earth and Environmental Science 14* (1), p. 012005. IOP Publishing

Gong, X., Zhang, X., Lohmann, G., Wei, W., Zhang, X., & Pfeiffer, M. (2015). Higher Laurentide and Greenland ice sheets strengthen the North Atlantic ocean circulation. *Climate Dynamics*, *45*(1–2), 139–150. https://doi.org/10.1007/s00382-015-2502-8

Groeneveld, J., and Chiessi, C. M. (2011). Mg/Ca of *Globorotalia inflata* as a recorder of permanent thermocline temperatures in the South Atlantic. *Paleoceanography*, *26* (PA2203), doi:10.1029/2010PA001940.

Grootes, P. M., Stuiver, M., White, J. W. C., Johnsen, S., & Jouzel, J. (1993). Comparison of oxygen isotope records from the GISP2 and GRIP Greenland ice cores. *Nature*, *366*(6455), 552–554. https://doi.org/10.1038/366552a0

Gwiazda, R. H., Hemming, S. R., & Broecker, W. S. (1996). Provenance of icebergs during Heinrich event 3 and the contrast to their sources during other Heinrich episodes. Paleoceanography, 11(4), 371-378.

Hayward, B.W. (2011). Globorotalia inflata. *World Register of Marine Species (WoRMS).* Retrieved from http://www.marinespecies.org/photogallery.php?album=772&pic=38452

Heinrich, H. (1988). Origin and Consequences of Cyclic Ice Rafting in the Northeast Atlantic Ocean During the Past 130,000 Years. *Quaternary Research*, *29*(2), 142–152. https://doi.org/10.1016/0033-5894(88)90057-9

Hodell., D.A., Nicholl, J.A., Bontognali, T.R.R., Danino, S., Dorador, J., Dowdeswell Einsle , J., Kuhlmann, H., Martrat, B., Mleneck-Vautravers, M.J.,Rodríguez-Tovar, F.J., & U. Röhl. (2017), Anatomy of Heinrich Layer 1 and its role in the last deglaciation, *Paleoceanography*, 32, 284–303, doi:10.1002/2016PA003028.

Hooper, P., & Weaver, P. (1987). *Paleoceanographic Significance of Late Miocene to Early Pliocene Planktonic Foraminifers at Deep Sea Drilling Project Site 609*. https://doi.org/10.2973/DSDP.PROC.94.129.1987

Johannessen, T., Jansen, E., Flatøy, A., & Ravelo, A.C. (1994). The relationship between surface water masses, oceanographic fronts and paleoclimatic proxies in surface sediments of the Greenland, Iceland and Norwegian Seas. *NATO ASI Series, 1* (17), 61-85

Katsman, C. A., Spall, M. A., & Pickart, R.S. (2004). Boundary Current Eddies and Their Role in the Restratification of the Labrador Sea. *Journal of Physical Oceanography*, *34*(9), 1967–1983. https://doi.org/10.1175/1520-0485(2004)034<1967:BCEATR>2.0.CO;2

Keigwin, L.D. and S. J. Lehman. (1994). Deep circulation change linked to HEINRICH event 1 and Younger Dryas in a middepth North Atlantic core. *Paleoceanographic Currents*, *9*(2), 185-194

Kipp, N.G. (1976). New transfer function for estimating past sea-surface conditions from sea-bed distribution of planktonic foraminiferal assemblages in the North Atlantic. *Geological Society of America, 145*, 3-41

Lehman, S. J., & Keigwin, L. D. (1992). Sudden changes in North Atlantic circulation during the last deglaciation. *Nature*, *356*(6372), 757–762. https://doi.org/10.1038/356757a0

Lisiecki, L. E., & Raymo, M. E. (2005). A Pliocene-Pleistocene stack of 57 globally distributed benthic δ18O records. *Paleoceanography*, *20* (1).

Locarnini R.A., Mishonov A.V, Antonov J.I, Boyer T.P, & H.E. Garcia. (2006). WorldOcean Atlas 2005, Volume 1: Temperature. *In: Levitus S, editor*, *NOAA AtlasNESDIS 61*, Washington, D.C.: U.S. Gov. Printing Office. p. 182. http://www.nodc.noaa.gov/OC5/indprod.html.

Lott, A. (2020). Hydrographic changes and Heinrich events in the Labrador Sea (Thesis). Columbia College, New York, NY, USA

MacAyeal, D. R. (1993). Binge/purge oscillations of the Laurentide ice sheet as a cause of the North Atlantic's Heinrich events. *Paleoceanography* 8.6, p.775-784.

Marchal, O., Waelbroeck, C., & Verdière, A. C. de. (2016). On the Movements of the North Atlantic Subpolar Front in the Preinstrumental Past. *Journal of Climate*, *29*(4), 1545–1571. https://doi.org/10.1175/JCLI-D-15-0509.1

Marzocchi, A., Hirschi, J. J.-M., Holliday, N. P., Cunningham, S. A., Blaker, A. T., & Coward, A. C. (2015). The North Atlantic subpolar circulation in an eddy-resolving global ocean model. *Journal of Marine Systems*, *142*, 126–143. https://doi.org/10.1016/j.jmarsys.2014.10.007

McManus, J. F., Anderson, R.F., Broecker, W.S., Fleisher, M.Q., & S.M. Higgins. (1998). Radiometrically determined sedimentary fluxes in the sub-polar North Atlantic during the last 140,000 years. *Earth Planet Science Letters*, 155, p. 29-43

McManus, J. F., Major, C.O., Flower, B.P., & Fronval, T. (1996). Variability in sea-surface conditions in the North Atlantic-Arctic Gateways during the last 140,000 years. *In* Thiede, J., Myhre, A.M., Firth, J.V., Johnson, G.L., and Ruddiman, W.F. (Eds.), *Proc. ODP, Sci. Results*: *College Station, TX (Ocean Drilling Program)*, 151, p. 437444. doi:10.2973/odp.proc.sr.151.131.1996

McManus, J. F., Oppo, D. W., & Cullen, J. L. (1999). A 0.5-Million-Year Record of Millennial-Scale Climate Variability in the North Atlantic. *Science*, *283*(5404), 971–975.

McManus, J. F., Oppo, D. W., Keigwin, L. D., Cullen, J. L., & Bond, G. C. (2002). Thermohaline Circulation and Prolonged Interglacial Warmth in the North Atlantic. *Quaternary Research*, *58*(1), 17–21. https://doi.org/10.1006/qres.2002.2367

McManus, J. F., Francois, R., Gherardi, J.-M., Keigwin, L. D., & Brown-Leger, S. (2004). Collapse and rapid resumption of Atlantic meridional circulation linked to deglacial climate changes. *Nature*, *428*(6985), 834–837. https://doi.org/10.1038/nature02494

Meese, D. A., Gow, A. J., Alley, R. B., Zielinski, G. A., Grootes, P. M., Ram, M., Taylor, K. C., Mayewski, P. A., & Bolzan, J. F. (1997). The Greenland Ice Sheet Project 2 depth-age scale: Methods and results. *Journal of Geophysical Research: Oceans*, *102*(C12), 26411–26423. https://doi.org/10.1029/97JC00269

Naafs, B. D. A., Hefter, J., Ferretti, P., Stein, R., & Haug, G. H. (2011). Sea surface temperatures did not control the first occurrence of Hudson Strait Heinrich Events during MIS 16. *Paleoceanography*, *26*(4). https://doi.org/10.1029/2011PA002135

Naafs, B.D.A, Hefter. J., Grüztner, J., & R. Stein. (2013). Warming of surface waters in mid-latitude North Atlantic during Heinrich Events. *Paleoceanography*, *28*, 153-163

O'Regan, M., Coxall, H.K., Cronin, T.M., Gyllencreutz, R., Jakobsson, M., Kaboth, S.,

Löwemark, L., Weirs, S., & G. West. (2019). Stratigraphic occurrences of sub-polar planktic foraminifera in PLeistocene sediments on the Lomonosov Ridge, Arctic Ocean. *Frontiers in Earth Science, 7*(71), 1-18

Pflaumann, U., Duprat, J., Pujol, C., & L.D. Labeyrie. (1996). SIMMAX: A modern analog technique to deduce Atlantic sea surface temperatures from planktonic foraminifera in deep-sea sediments. *Paleoceanography, 11*(1), 15-35

Pflaumann, U., Sarnthein, M., Chapman, M., d'Abreu, L., Funnell, B., Huels, M., Keifer, T., Malsin, M., Schulz, H., Swallow, J., van Kreveld, S., Vautravers, M., Vogelsang, E., & M. Weinelt. (2003). Glacial North Atlantic: sea-surface conditions reconstructed by GLAMAP 2000. *Paleoceanography, 18*(3), 1-28

Ronnfeld, W. (2007). Light-microscope image of the san-fraction residue from a tropical deep-sea sediment sample (20 species represented)[Image] in Kucera, M. (2007). *Chapter Six Planktonic Foraminifera as Tracers of Past Oceanic Environments*. https://doi.org/10.1016/S1572-5480(07)01011-1

Ruddiman, W.F. (1977a). Late Quaternary deposition of ice-rafted sand in the subpolar North Atlantic (lat 40 to 65 N). *Geological Society of America Bulletin, 88,* 1813-1827.

Ruddiman, W. F. (1977b). North Atlantic Ice-Rafting: A Major Change at 75,000 Years Before the Present. *Science, 196*(4295), 1208–1211.

Sancetta, C. (1992). Primary production in the glacial North Atlantic and North Pacific oceans. *Nature, 360*(6401), 249–251. https://doi.org/10.1038/360249a0

Stanley, S. (2017). Iceberg surge during the last deglaciation may have had two pulses. *Eos, 98,* https://doi.org/10.1029/2017EO071933. Published on 27 April 2017

Stouffer, R. J., Yin, J., Gregory, J. M., Dixon, K. W., Spelman, M. J., Hurlin, W., Weaver, A. J., Eby, M., Flato, G. M., Hasumi, H., Hu, A., Jungclaus, J. H., Kamenkovich, I. V., Levermann, A., Montoya, M., Murakami, S., Nawrath, S., Oka, A., Peltier, W. R., … Weber, S. L. (2006). Investigating the Causes of the Response of the Thermohaline Circulation to Past and Future Climate Changes. *Journal of Climate*, *19*(8), 1365–1387. https://doi.org/10.1175/JCLI3689.1

Taylor, J.R. (1982). *An Introduction to Error Analysis: The study and uncertainties in physical measurements*. Sausalito, USA: University Science Books.

University of Washington. (2002). Climate and Climate Change (ATM S 211, Winter Quarter). *College of the Environment* [Lecture notes]. https://atmos.washington.edu/academics/classes/2002Q1/211/notes_marinebiosphere.html

United States Geological Survey (USGS). (2009). Debris covered iceberg calved from terminus of Alaska's Sheridan Glacier [Image]. *USGS, American Geological Institute, https://upload.wikimedia.org/wikipedia/commons/7/79/Hflu9n.jpg*

Zahn, R., Shönfeld, J., Kudrass, H.R., Park, M. H., Erlenkeuser, H., & P. Grootes. (1997). Thermohaline instability in the North Atlantic during meltwater events: Stable isotope and ice-rafted detritus records from core SO75-26KL, Portuguese margin, *Paleoceanography, 12*(5), 696-710. https://doi.org/10.1029/97PA00581